Patient management

After intubation, all patients were subjected to continuous mild hyperventilation, which was induced with $Paco_2$ between 30 and 35 mmHg, and all received high-dose barbiturates with mild fluid restriction (1–2 mL/kg/h). On reaching cerebral perfusion pressure (mean arterial blood pressure minus ICP) of less than 60 mmHg, patients were given adequate amounts of albumin. Colloidal fluids or dopamine (3–5 μg/kg/min continuous infusion) was administered as needed to maintain urine output greater than 0.5 mL/kg/h. No corticosteroid or mannitol was administered during the study. Immediately after initial resuscitation, all patients underwent computed tomography (CT) scanning of the head. Subsequently, an intraventricular catheter was placed in each patient. The catheter allowed continuous monitoring of ICP and intracranial temperature. There was no evidence of complications, such as intracranial hemorrhage or infection, as a result of insertion of the intraventricular catheter. Intracranial mass lesions associated with midline displacement greater than 5 mm were surgically removed when necessary. Intracranial hypertension was managed initially in all patients by conventional ICP reduction therapy, such as mild hyperventilation, mild fluid restriction, high-dose barbiturates, and/or CSF drainage. In patients with ICP at or above 20 mmHg and unresponsive to conventional therapy, mild hypothermia (34°C) was induced by surface cooling with a circulating water blanket placed above and below the patient. Intracranial temperature was controlled according to our previously published protocol (24). Control of ICP was achieved in 17 of the 23 patients (low-ICP group) but not in the remaining 6 (high-ICP group). Patients in the low-ICP group were assigned randomly to mild hypothermia (HT, 11 patients) or normothermia (NT, 6 patients). After randomization, HT patients were subjected to mild hypothermia (intracranial temperature = 34°C) as quickly as possible, and NT patients were maintained under normothermic conditions (intracranial temperature = 37°C). Mild hypothermia was started 2.0 ± 0.5 h after injury, and body temperature reached 34°C 6.0 ± 0.5 h after injury. Mild hypothermia was continued for 48 h, and patients were rewarmed at 1°C /day for 3 days. Normothermia (37°C) was maintained for 5 days.

CT study

Focal mass lesions included contusion, subdural hematoma, epidural hematoma, and intracerebral hematoma. Volume measurements of focal mass lesions based on CT images taken during the first 24 h after TBI were obtained according to Cavalieri's Direct Estimator method (25).

CSF and serum analysis

CSF samples were drawn from the intraventricular catheter, and blood samples were drawn from an arterial line immediately after insertion of the intraventricular catheter (initial sampling time was 2.0 ± 0.5 h after injury) and at 6, 12, 24, 48, 72, and 96 h after injury. The CSF samples were centrifuged to remove cellular debris, and the supernatant was immediately frozen at −80°C and stored until analysis. Serum samples were prepared from the blood samples and stored at −80°C until analysis. TNF-α, IL-1β, IL-6, IL-8, and IL-10 concentrations in CSF and serum were analyzed by enzyme-linked immunosorbent assay with commercially available kits (R&D Systems, Minneapolis, MN). The minimum detectable cytokine concentrations were TNF-α 4.4 pg/mL, IL-1β 1 pg/mL, IL-6 0.7 pg/mL, IL-8 10 pg/mL, and IL-10 3.9 pg/mL. For statistical analysis, minimum-detection-level values were used for cytokine concentrations below the minimum detectable levels. CSF S100B concentrations were determined with a commercially available immunoradiometric assay kit (Sangtec Medical, Bromma, Sweden). CSF samples obtained by diagnostic lumbar puncture from seven trauma patients without traumatic brain injury were used as controls.

Patient outcomes

Patient outcome was assessed 6 months after injury on the basis of the Glasgow Outcome Scale (GOS) (26) in which death is scored as 1, vegetative state as 2, severe disability as 3, moderate disability as 4, and good recovery as 5. For statistical comparison, the outcomes of patients with scores of 4 or 5 were considered favorable, and the outcomes of patients with scores of 1, 2, or 3 were considered unfavorable. Surviving patients participated in follow-up interviews either by telephone or in person at the clinic.

Statistical analysis

All values are expressed as mean ± standard error of the mean unless otherwise specified. Statistical analyses were performed with Stat-View computer software (version 5.0) and included Mann-Whitney *U* test, chi-square test, or one-way analysis of variance in combination with the Tukey-Kramer multiple comparisons test. Relations between variables were assessed by Pearson's correlation coefficient. Differences were considered statistically significant at $P < 0.05$.

RESULTS

Patients' characteristics

Of the 23 patients, six made up the "patients with low ICP treated under normothermia" group (NT group), 11 made up the "patients with low ICP treated under mild hypothermia" group (HT group), and six made up the "patients with high ICP" group. All patients with high ICP were treated under mild hypothermia. We had no patients with high ICP treated under normothermia. Clinical characteristics in the three groups are

TABLE 1. **Clinical characteristics of the three study groups**

	Patients with low ICP* treated under normothermia (NT group)	Patients with low ICP* treated under mild hypothermia (HT group)	Patients with high ICP†
No. of patients	6	11	6
Age (yrs)	34 ± 7	37 ± 6	49 ± 8
Sex ratio (M/F)	3/3	11/0	3/3
GCS on admission	5.8 ± 0.8	5.9 ± 0.5	5.0 ± 0.3
CT classification§			
Diffuse injury 1	1	0	0
Diffuse injury 2	3	7	0
Diffuse injury 3	0	0	1
Diffuse injury 4	0	0	0
Evacuated mass lesion	2	4	5
Nonevacuated mass lesion	0	0	0
Additional injuries			
Chest injury	2	1	2
Abdominal injury	0	2	0
Pelvic or leg fracture	0	0	1
Arm fracture	0	0	0
Outcome			
Favorable/unfavorable	6/0	8/3	1/5

Numbers represent number of patients unless otherwise indicated.
Values are expressed as mean ± standard error of the mean.
*Low ICP, patient's ICP was maintained below 20 mmHg by conventional treatments. There were no significant differences between the two groups.
†High ICP, patient's ICP could not be lowered to below 20 mmHg despite conventional treatments. All patients with high ICP were treated under mild hypothermia.
§Categorized according to the classification of Marshall et al. (34).

summarized in Table 1. There were no significant differences between the NT group and the HT group in age, GCS score on admission, focal mass volume, additional injuries, or outcome.

CSF S100B and cytokine concentrations in patients with severe TBI

The mean peak CSF S100B concentration (630 ± 173 μg/L) of the 23 patients with severe TBI was much higher than that (3.3 ± 1.3 μg/L) of the control patients ($P < 0.001$) (Fig. 1). The mean peak CSF cytokine concentrations of the 23 patients were IL-1β 9.9 ± 1.7 pg/mL, TNF-α 23.0 ± 5.7 pg/mL, IL-6 5266 ± 1633 pg/mL, IL-8 12,602 ± 2,115 pg/mL, and IL-10 12.6 ± 2.3 pg/mL. However, the mean CSF cytokine concentrations of the control patients were 1.6 ± 0.2 pg/mL for IL-1β, 11.9 ± 5.0 pg/mL for IL-6, and 96.2 ± 4.3 pg/mL for IL-8. CSF TNF-α and IL-10 concentrations were undetectable in the control patients. All peak CSF cytokine concentrations were significantly higher in the 23 patients with severe TBI than in the control patients ($P < 0.05$) (Fig. 1).

Serial changes in CSF S100B and cytokine concentrations

CSF S100B concentrations increased during the 6-h period immediately after injury and gradually decreased thereafter (Fig. 2A). CSF IL-1β and -α concentrations were substantially higher than those of control patients during the 24-h period immediately after TBI, and they decreased thereafter (Fig. 2, B and C). CSF IL-6 and IL-8 concentrations peaked 6 h after injury and decreased gradually thereafter (Fig. 2, D and E), whereas the CSF IL-10 concentration was substantially higher during the 6-h period immediately after injury but decreased steadily after the initial sampling time (Fig. 2F). During the first 24 h after injury, IL-1β, TNF-α, IL-6, and IL-8 concentrations were two to 100 times higher in CSF than in serum. However, the CSF concentration of IL-10 was lower than the serum concentration.

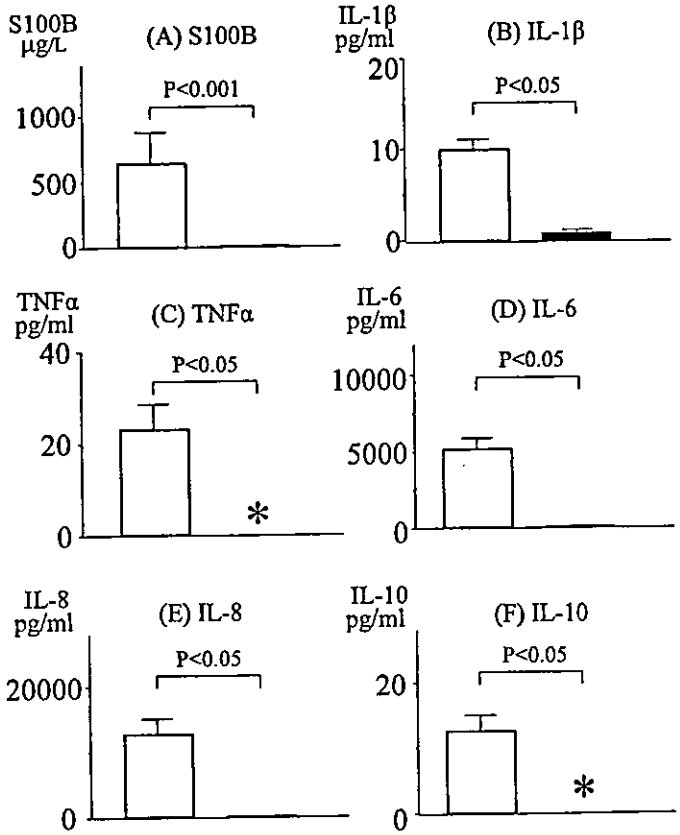

FIG. 1. **Graphs showing peak CSF concentrations of S100B (A) and cytokines (B–F) in 23 patients with severe TBI and controls.** Open bars, patients with severe TBI. Closed bars, control patients. Data are expressed as mean ± SEM values. *CSF TNF-α and IL-10 concentrations were undetectable in the control patients.

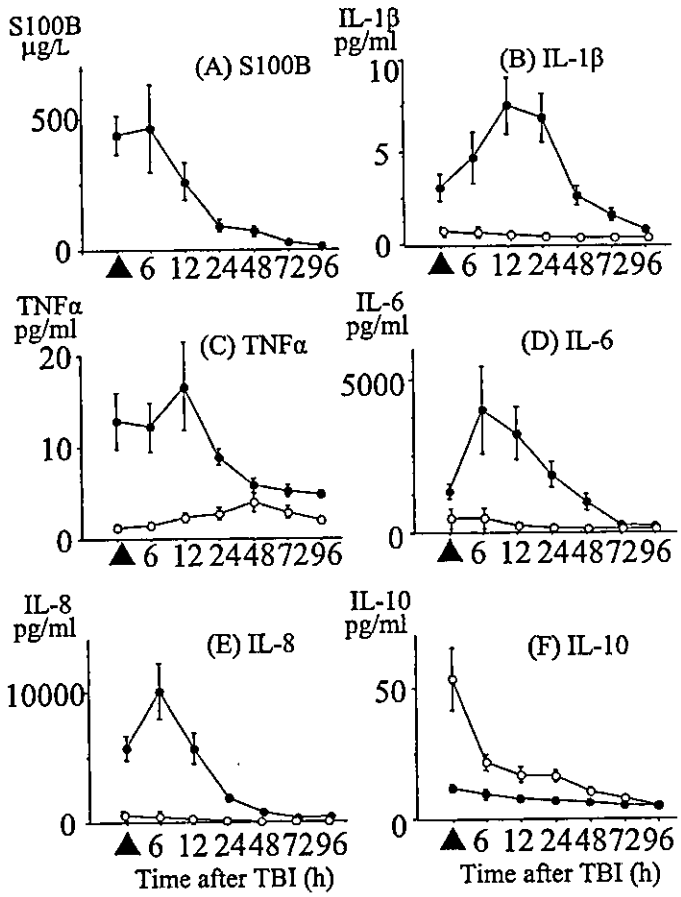

FIG. 2. **Graphs showing serial changes in CSF S100B concentration (A) and serial changes in CSF and serum cytokine concentrations (B–F) in 23 patients with severe TBI.** Data are expressed as mean ± SEM values. ▲, Initial sampling time for CSF and serum; ●, CSF S100B and cytokine concentrations; ○, serum cytokine concentrations.

Correlation of ICP with S100B and cytokines

A positive correlation ($r^2 = 0.729$, $P < 0.0001$) was found between peak CSF S100B concentration and ICP at each sampling point (Fig. 3). The CSF S100B concentration was significantly higher in the high-ICP group than in the low-ICP group ($P < 0.001$, Table 2). A significant correlation was found between peak CSF IL-1β concentration and ICP at each sampling point ($r^2 = 0.260$, $P < 0.05$). The CSF IL-1β concentration was also significantly higher in the high-ICP group than in the low-ICP group ($P < 0.05$). No significant correlation was found between other peak CSF cytokine concentrations and ICP at any sampling point.

Serial changes in CSF S100B and cytokine concentrations in HT and NT groups

Serial changes in CSF S100B and cytokine concentrations in the HT group did not differ statistically from changes in the NT

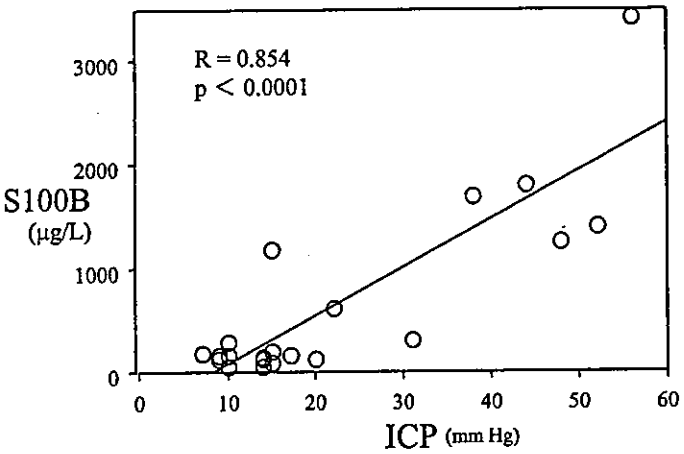

FIG. 3. **Graph showing correlation between ICP and peak CSF S100B concentration in the 23 study patients with severe TBI.** Measurements of ICP and sampling of CSF for S100B assay were done at the same time.

group (Fig. 4). These two groups did not differ significantly in age, GCS score on admission, focal mass volume, level of ICP, additional injuries, or outcome (Table 1).

Correlation of GCS score with S100B and cytokines

No significant correlation was found between the peak CSF S100B concentration and a patient's GCS score on admission. Nor was a significant correlation found between the peak CSF cytokine concentrations and a patient's GCS score on admission.

Correlation of focal mass volume with S100B and cytokines

Significant positive correlation was found between peak CSF S100B concentration and focal mass volume ($r^2 = 0.316$, $P < 0.005$). However, no significant correlations were found between peak CSF cytokine concentrations and focal mass volume.

Correlation between peak CSF S100B and cytokine concentrations

Significant positive correlation ($r^2 = 0.397$, $P < 0.005$) was found between peak CSF S100B concentration and peak CSF IL-1β concentration in the overall study group (Fig. 5). However, no significant correlation was detected between peak CSF concentration of any other cytokine and peak CSF concentration of S100B.

Peak CSF S100B and cytokine concentrations and outcome

At 6 months after TBI, outcome was favorable for 15 patients but unfavorable for eight patients (Table 1). The CSF S100B concentration was significantly higher in patients with an unfavorable outcome than in patients with a favorable outcome ($P < 0.05$) (Table 3). The CSF IL-1β concentration tended to be higher in patients with an unfavorable outcome than in patients with a favorable outcome ($P = 0.057$) (Table 3). No differences were found in CSF concentrations of other cytokines between patients with a favorable outcome and those with an unfavorable outcome (Table 3).

DISCUSSION

In patients with severe TBI, the serum S100B concentration is high on admission, and it decreases gradually (27). However, the changes in CSF S100B that occur early in patients with severe TBI are not clearly understood. The present study showed clearly that the CSF S100B concentration peaked within 6 h after injury and that the peak CSF S100B concentration correlated significantly with ICP determined at the time CSF samples were taken. The mean peak CSF S100B concentration (630 ± 173 μg/L) of the 23 patients with severe TBI was much higher than that (3.3 ± 1.3 μg/L) of the control patients ($P < 0.001$). CSF values from our control subjects were slightly higher than that (1.4 ± 0.2 μg/L) reported by Pleines et al. (7), but we think the actual differences were really very small. Our findings are consistent with those of Hardemark et al. (28), who reported that the CSF S100B concentration peaked 7.5 h after experimental traumatic brain injury in the rat. Hardemark et al. (28) concluded that TBI causes astroglial cells to rupture; thus, the early peak of S100B in CSF may reflect primary brain damage.

Several authors have reported increased serum concentrations of S100B in TBI patients (3–6). Woertgen et al. reported that the serum S100B concentration was significantly higher in patients with an unfavorable outcome than in patients with a favorable outcome (29). Raabe et al. reported a significant correlation between the serum S100B concentration and contusion volume determined from CT scans (30). With respect to TBI, some authors have shown a related increase in S100B in CSF (7, 8, 31). However, details concerning the correlation between CSF S100B concentration and prognosis in patients with severe TBI are not sufficiently understood. In our study, the CSF S100B concentration was significantly higher in patients with an unfavorable outcome than in patients with a favorable outcome. Moreover, the CSF S100B concentration correlated with ICP and with focal mass lesion volume. We believe, therefore, that CSF S100B concentration provides greater prognostic value than serum S100B concentration in the treatment of severe TBI patients.

Early increases in various cytokines in the brain have been reported in rat brain injury models. Reports show that cytokines such as TNF-α, IL-1β, and IL-6 increase, peak within a few hours after brain injury, and then decrease (10, 11). In humans, TBI causes release of various cytokines into the CSF (16, 17, 20, 21). However, in the clinical studies, analysis of cytokine concentrations was performed only on a daily basis, and early changes (within 24 hours) in CSF cytokines in patients with TBI have not been well documented. Like earlier studies in animal models, our study clearly indicated that CSF concentrations of cytokines IL-6 and IL-8 peaked by 6 h after injury, and CSF concentrations of cytokines IL-1β, TNF-α, and IL-10 increased within the first 24 h after injury. Interestingly, CSF concentrations of IL-1β, TNF-α, IL-6, and IL-8 were markedly higher than serum concentrations of these cytokines in our patients. These results are consistent with those of Maier et al. (22), who reported that concentrations of IL-6 and IL-8 were much higher in the CSF than in the plasma of TBI patients. They also found that alterations in the blood–brain

TABLE 2. Peak concentrations of CSF S100B and CSF cytokines in TBI patients based on intracranial pressure (ICP)

	S100B (μg/L)	IL-1β (pg/mL)	TNFα (pg/mL)	IL-6 (pg/mL)	IL-8 (pg/mL)	IL-10 (pg/mL)
Patients with high ICP* (n = 6)	1649 ± 415	16.5 ± 3.3	27.1 ± 18.6	5767 ± 1556	6,802 ± 2513	18.1 ± 7.3
Patients with low ICP† (n = 17)	233 ± 67	7.6 ± 1.6	20.8 ± 4.7	5090 ± 2165	14,649 ± 2573	10.7 ± 1.8
P value	$P < 0.001$	$P < 0.05$	$P = 0.195$	$P = 0.207$	$P = 0.092$	$P = 0.483$

Values are expressed as mean ± standard error of the mean.
*High ICP, patient's ICP could not be lowered to below 20 mmHg despite conventional treatments.
†Low ICP, patient's ICP was maintained below 20 mmHg by conventional treatments.
P value obtained by Mann-Whitney *U* test for the difference between the two groups.

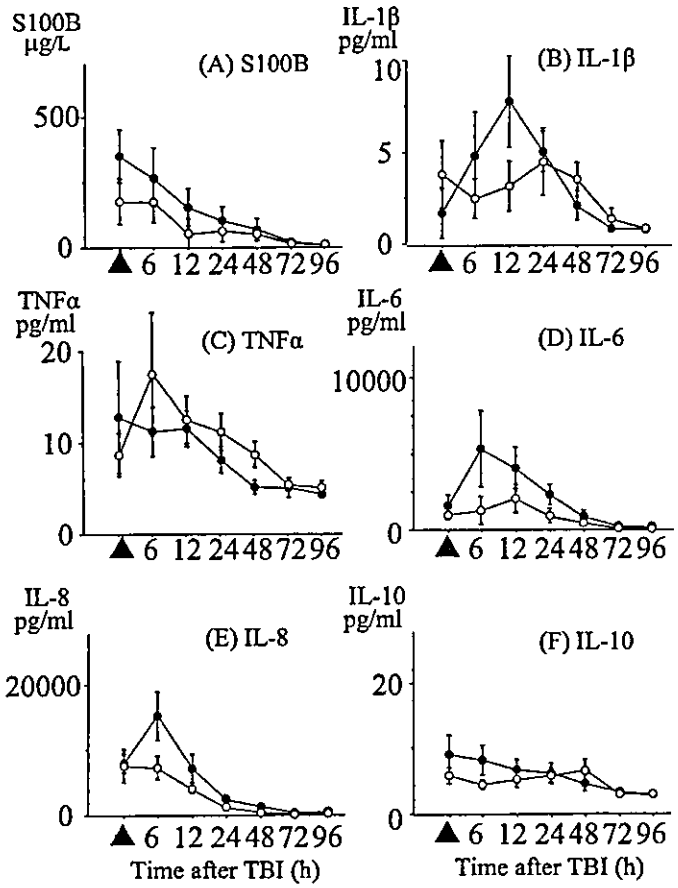

FIG. 4. Graphs showing serial changes in CSF S100B concentration (A) and serial changes in CSF cytokine concentrations (B–F) in HT group patients (●, n = 11) and NT group patients (○, n = 6). Data are expressed as mean ± SEM values. ▲, initial sampling time for CSF. There were no significant differences between the two groups.

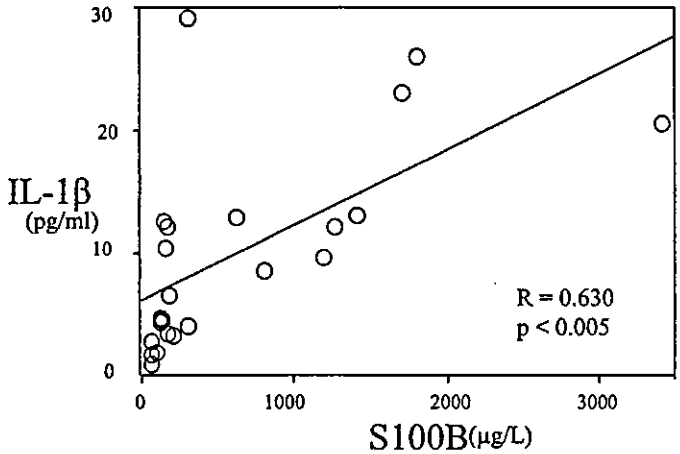

FIG. 5. Graph showing correlation between peak CSF S100B concentration and peak CSF IL-1β concentration in the 23 study patients with severe TBI.

barrier seemed not to influence the distribution of cytokines in CSF and plasma after TBI (22). We therefore speculate that these cytokines originate from neurons, microglia, and astrocytes. However, the means by which the excessively increased IL-1β, TNF-α, IL-6, and IL-8 in CSF act in mediating the inflammatory response remain unclear. The relationship between the cerebral inflammatory response and the systemic inflammatory response is yet to be clarified. In contrast to these proinflammatory cytokines, anti-inflammatory IL-10 was concentrated less in CSF than in serum throughout most of the study period. This peculiar distribution of IL-10 was consistent with that reported by Maier et al. (22). We are now investigating the cause of this notable disproportion between inflammatory mediators and anti-inflammatory mediators after TBI.

Barbiturate therapy and mild hypothermia were used in our patients. Barbiturate administration induces human mononuclear leukocytes to release cytokines (32), and S100B may be released by this agent (33). However, whether barbiturate is associated with the increase of S100B and cytokines in the CSF of patients with brain injury could not be determined in this study because all 23 patients received high-dose barbiturates. Although hypothermia has been reported to suppress cytokine production in patients with TBI (22), we found no difference in the serial changes in cytokine concentrations between patients treated under hypothermia and those treated under normothermia.

There are several limitations to our study. First, it may be argued that the number of patients was small and that it is therefore difficult to confirm the relationship between the type of TBI and CSF concentrations of S100B and cytokines. Second, we can not clarify to what degree the increase in CSF S100B and cytokines reflects the extent of ongoing brain damage because it is not ethically feasible to perform CT scanning every 6 h. Third, we can not ascertain serial changes in CSF concentrations of S100B and cytokines because it is difficult to collect CSF samples every 1 or 2 h in the clinical setting. From the present study, therefore, we can not clarify whether the increase in CSF S100B directly induces the increase in CSF IL-1β or leads indirectly to the increase in CSF IL-1β.

We measured CSF concentrations of S100B and cytokines simultaneously during the initial 96 h after severe TBI. The CSF S100B concentration peaked in the early phase of severe TBI, and CSF cytokine concentrations also increased during the early phase or promptly after the CSF S100B elevation.

TABLE 3. Peak CSF S100B and cytokine concentrations in the TBI patients per outcome

	S100B (μg/L)	IL-1β (pg/mL)	TNFα (pg/mL)	IL-6 (pg/mL)	IL-8 (pg/mL)	IL-10 (pg/mL)
Unfavorable* (n = 8)	1231 ± 378	14.8 ± 3.4	12.1 ± 2.0	4452 ± 1022	9266 ± 3384	17.8 ± 5.9
Favorable† (n = 15)	267 ± 108	7.3 ± 1.5	28.9 ± 8.3	5701 ± 2472	14,381 ± 2660	9.9 ± 1.6
P value	*P* < 0.05	*P* = 0.057	*P* = 0.155	*P* = 0.561	*P* = 0.155	*P* = 0.388

Values are expressed as mean ± standard error of the mean.
*Patients with a GOS score of 1, 2, or 3.
†Patients with a GOS score of 4 or 5.
P value obtained by Mann-Whitney *U* test for the difference between the two groups.

Only the CSF IL-1β concentration correlated with the CSF S100B concentration. However, we could not uncover the reason for this correlation. Further study is needed to clarify the precise relationship between CSF S100B and CSF IL-1β in severe TBI.

REFERENCES

1. Zimmer DB, Cornwall EH, Landar A, Song W: The S100 protein family: history, function, and expression. *Brain Res Bull* 37:417–429, 1995.
2. Bianchi R, Garbuglia M, Verzini M, Giambanco I, Ivanenkov VV, Dimlich RV, Jamieson GA Jr, Donato R: S-100 (alpha and beta) binding peptide (TRTK-12) blocks S-100/GFAP interaction: identification of a putative S-100 target epitope within the head domain of GFAP. *Biochim Biophys Acta* 1313:258–267, 1996.
3. Biberthaler P, Mussack T, Wiedemann E, Gilg T, Soyka M, Koller G, Pfeifer KJ, Linsenmaier U, Mutschler W, Gippner-Steppert C, Jochum M: Elevated serum levels of S-100B reflect the extent of brain injury in alcohol intoxicated patients after mild head trauma. *Shock* 16:97–101, 2001.
4. Pelinka LE, Toegel E, Mauritz W, Redl H: Serum S 100 B: a marker of brain damage in traumatic brain injury with and without multiple trauma. *Shock* 19: 195–200, 2003.
5. Biberthaler P, Mussack T, Wiedemann E, Kanz KG, Koelsch M, Gippner-Steppert C, Jochum M: Evaluation of S-100b as a specific marker for neuronal damage due to minor head trauma. *World J Surg* 25:93–97, 2001.
6. Mussack T, Biberthaler P, Gippner-Steppert C, Kanz KG, Wiedemann E, Mutschler W, Jochum M: Early cellular brain damage and systemic inflammatory response after cardiopulmonary resuscitation or isolated severe head trauma: a comparative pilot study on common pathomechanisms. *Resuscitation* 49:193–199, 2001.
7. Pleines UE, Morganti-Kossmann MC, Rancan M, Joller H, Trentz O, Kossmann T: S-100 beta reflects the extent of injury and outcome, whereas neuronal specific enolase is a better indicator of neuroinflammation in patients with severe traumatic brain injury. *J Neurotrauma* 18:491–498, 2001.
8. Berger RP, Pierce MC, Wisniewski SR, Adelson PD, Clark RS, Ruppel RA, Kochanek PM: Neuron-specific enolase and S100B in cerebrospinal fluid after severe traumatic brain injury in infants and children. *Pediatrics* 109:E31, 2002.
9. Rothermundt M, Peters M, Prehn JH, Arolt V: S100B in brain damage and neurodegeneration. *Microsc Res Tech* 60:614–632, 2003.
10. Shohami E, Novikov M, Bass R, Yamin A, Gallily R: Closed head injury triggers early production of TNFα and IL-6 by brain tissue. *J Cereb Blood Flow Metab* 14:615–619, 1994.
11. Taupin V, Toulmond S, Serrano A, Benavides J, Zavala F: Increase in IL-6, IL-1 and TNF levels in rat brain following traumatic lesion. Influence of pre- and post-traumatic treatment with Ro5 4864, a peripheral-type (*p* site) benzodiazepine ligand. *J Neuroimmunol* 42:177–185, 1993.
12. Gaetani P, Tartara F, Pignatti P, Tancioni F, Rodriguez y Baena R, De Benedetti F: Cisternal CSF levels of cytokines after subarachnoid hemorrhage. *Neurol Res* 20:337–342, 1998.
13. Tarkowski E, Rosengren L, Blomstrand C, Wikkelso C, Jensen C, Ekholm S, Tarkowski A: Intrathecal release of pro- and anti-inflammatory cytokines during stroke. *Clin Exp Immunol* 110:492–499, 1997.
14. Otto L, Mcclain CJ, Gillespie M, Young B: Cytokines and metabolic dysfunction after severe head injury. *J Neurotrauma* 11:447–472, 1994.
15. Morganti-Kossmann MC, Rancan M, Otto VI, Stahel PF, Kossmann T: Role of cerebral inflammation after traumatic brain injury: a revisited concept. *Shock* 16:165–177, 2001.
16. Bell MJ, Kochanek PM, Doughty LA, Carcillo JA, Adelson PD, Clark RS, Wisniewski SR, Whalen MJ, DeKosky ST: Interleukin-6 and interleukin-10 in cerebrospinal fluid after severe traumatic brain injury in children. *J Neurotrauma.* 14:451–457, 1997.
17. Kossmann T, Hans V, Imhof HG, Trentz O, Morganti-Kossmann MC: Interleukin-6 released in human cerebrospinal fluid following traumatic brain injury may trigger nerve growth factor production in astrocytes. *Brain Res* 713:143–152, 1996.
18. Marion DW, Penrod LE, Kelsey SF, Obrist WD, Kochanek PM, Palmer AM, Wisniewski SR, DeKosky ST: Treatment of traumatic brain injury with moderate hypothermia. *N Engl J Med* 336:540–546, 1997.
19. Vos PE, Verbeek MM: Brain specific proteins in serum: Do they reliably reflect brain damage? *Shock* 18:481–482, 2002.
20. Csuka E, Morganti-Kossmann MC, Lenzlinger PM, Joller H, Trentz O, Kossmann T: IL-10 levels in cerebrospinal fluid and serum of patients with severe traumatic brain injury: relationship to IL-6, TNF-α, TGF-ββα1 and blood–brain barrier function. *J Neuroimmunol* 101:211–221, 1999.
21. Kossmann T, Stahel PF, Lenzlinger PM, Redl H, Dubs RW, Trentz O, Schlag G, Morganti-Kossmann MC: Interleukin-8 released into the cerebrospinal fluid after brain injury is associated with blood–brain barrier dysfunction and nerve growth factor production. *J Cereb Blood Flow Metab* 17:280–289, 1997.
22. Maier B, Schwerdtfeger K, Mautes A, Holanda M, Muller M, Steudel WI, Marzi I: Differential release of interleukins 6, 8, and 10 in cerebrospinal fluid and plasma after traumatic brain injury. *Shock* 15:421–426, 2001.
23. Teasdale G, Jennett B: Assessment of coma and impaired consciousness. A practical scale. *Lancet* 2:81–84, 1974.
24. Shiozaki T, Kato A, Taneda M, Hayakata T, Hashiguchi N, Tanaka H, Shimazu T, Sugimoto H: Little benefit from mild hypothermia therapy for severely head injured patients with low intracranial pressure. *J Neurosurg* 91:185–191, 1999.
25. Clatterbuck RE, Sipos EP: The efficient calculation of neurosurgically relevant volumes from computed tomographic scans using Cavalieri's Direct Estimator. *Neurosurgery* 40:339–342, 1997.
26. Jennett B, Bond M: Assessment of outcome after severe brain damage. A practical scale. *Lancet* 1:480–484, 1975.
27. Woertgen C, Rothoerl RD, Holzschuh M, Metz C, Brawanski A: Comparison of serial S-100 and NSE serum measurement after severe head injury. *Acta Neurochir (Wien)* 139:1161–1165, 1997.
28. Hardemark HG, Ericsson N, Kotwica Z, Rundstrom G, Mendel-Hartvig I, Olsson Y, Pahlman S, Persson L: S-100 protein and neuron-specific enolase in CSF after experimental traumatic or focal ischemic brain damage. *J Neurosurg* 71:727–731, 1989.
29. Woertgen C, Rothoerl RD, Metz C, Brawanski A: Comparison of clinical, radiologic, and serum marker as prognostic factors after severe head injury. *J Trauma* 47:1126–1130, 1999.
30. Raabe A, Grolms C, Keller M, Dohnert J, Sorge O, Seifert V: Correlation of computed tomography findings and serum brain damage markers following severe head injury. *Acta Neurochir (Wien)* 140:787–792, 1998.
31. Persson L, Hardemark H, Edner G, Ronne E, Mendel-Hartvig I: Pahlman S: S-100 protein in cerebrospinal fluid of patients with subarachnoid haemorrhage: a potential marker of brain damage. *Acta Neurochir (Wien)* 93:116–122, 1988.
32. Rossano F, Tufano R, Cipollaro de L'Ero G, Servillo G, Baroni A, Tufano MA, Servillo G, Baroni A, Tufano MA: Anesthetic agents induce human mononuclear leucocytes to release cytokines. *Immunopharmacol Immunotoxicol* 14:439–450, 1992.
33. Rickmann M, Wolff JR: Modifications of S100-protein immunoreactivity in rat brain induced by tissue preparation. *Histochem Cell Biol* 103:135–145, 1995.
34. Marshall LF, Marshall SB, Klauber MR, Clark MB: A new classification of head injury based on computerized tomography. *J Neurosurg* 75:S14–S20, 1991.

ORIGINAL ARTICLE

Annals of Nuclear Medicine Vol. 18, No. 1, 35–44, 2004

PET measurements of CBF, OEF, and $CMRO_2$ without arterial sampling in hyperacute ischemic stroke: Method and error analysis

Masanobu IBARAKI,* Eku SHIMOSEGAWA,* Shuichi MIURA,* Kazuhiro TAKAHASHI,* Hiroshi ITO,* Iwao KANNO* and Jun HATAZAWA**

*Department of Radiology and Nuclear Medicine, Akita Research Institute, of Brain and Blood Vessels
**Division of Tracer Kinetics and Nuclear Medicine, Osaka University Graduate School of Medicine

A method for relative measurement of cerebral blood flow (CBF), oxygen extraction fraction (OEF), and metabolic rate of oxygen ($CMRO_2$) using positron emission tomography (PET) without arterial sampling in patients with hyperacute ischemic stroke was presented. ***Methods:*** The method requires two PET scans, one for $H_2{}^{15}O$ injection and one for ${}^{15}O_2$ inhalation, and calculates regional CBF, $CMRO_2$, and OEF relative to those at the reference brain region by means of table-lookup method. In this study, we calculated "relative lookup-tables" which relate relative CBF to relative $H_2{}^{15}O$ count, relative $CMRO_2$ to relative ${}^{15}O_2$ count, and relative OEF to relative ${}^{15}O_2/H_2{}^{15}O$ count. Two assumptions were applied to the lookup-table calculation: 1) In the reference region, CBF and OEF were assumed to be 50.0 m*l*/min/100 m*l* and 0.40, respectively, 2) Cerebral blood volume (CBV) was assumed to be constant at 4.0 m*l*/100 m*l* over the whole brain. Simulation studies were done to estimate the error of the present method derived from the assumptions. ***Results:*** For relative CBF measurements, 20% variation in reference CBF gave about ±10% error for measured relative CBF at maximum. Changes in CBV caused relatively large errors in measured OEF and $CMRO_2$ when relative CBF and OEF decreased. Errors for measured relative OEF caused by 50% variation in CBV were within ±8% at 0.8 of relative CBF and ±12% at 0.4 of relative CBF when relative OEF was greater than 1.0. ***Conclusion:*** CBV effects caused larger errors in estimated OEF and $CMRO_2$ in the region of the ischemic core with decreasing relative CBF and/or OEF but only slight errors in the region of "misery perfusion" with relative OEF values greater than 1.0. The present method makes PET measurements simpler than with the conventional method and increases understanding of the cerebral circulation and oxygen metabolism in patients with hyperacute stroke of several hours after onset.

Key words: PET, relative measurement, cerebral blood flow, oxygen metabolism, hyperacute stroke

INTRODUCTION

EFFECTIVE TREATMENT for patients with hyperacute ischemic stroke requires urgent and accurate diagnosis of brain ischemia and ischemic injury in the emergency setting.[1,2] Measurement of cerebral blood flow (CBF) in the hyperacute stage of cerebral infarction with single photon emission computed tomography (SPECT) has been used to estimate the CBF threshold for subsequent infarction,[3] and to predict the probability of hemorrhagic complications after acute thrombolytic therapy.[4–6] Although these SPECT-CBF were normalized by reference CBF of the unaffected cerebral or cerebellar hemisphere instead of using absolute values, relative CBF threshold provided reliable signposts for the diagnosis and treatment of the hyperacute stage of cerebral infarction. In addition to CBF, measurements of brain metabolism are also strongly

Received May 29, 2003, revision accepted October 27, 2003.
For reprint contact: Masanobu Ibaraki, Ph.D., Department of Radiology and Nuclear Medicine, Akita Research Institute of Brain and Blood Vessels, 6–10 Senshu-Kubota Machi, Akita 010–0874, JAPAN.
E-mail: iba@akita-noken.go.jp

needed to provide more accurate information on the brain tissue and the applicability of therapy. Positron emission tomography (PET) has made possible the quantification of CBF, oxygen extraction fraction (OEF), and cerebral metabolic rate of oxygen ($CMRO_2$).[7–10] The OEF and $CMRO_2$ can indicate the area with a risk of evolving infarction. Although these metabolic-related images can be measured only by PET, the clinical use of PET study in the emergency setting is not feasible because of the relatively time-consuming method needed for quantification. Arterial cannulation for the blood sampling adds time and is sometimes impossible. Derdeyn et al. recently applied a count-based PET method to estimate OEF for prediction of ischemic stroke in patients with symptomatic carotid artery occlusion.[11,12] This method was first used by Jones et al.[13] and requires no arterial sampling. Although their studies showed a great prospect of clinical PET usage,[11,12] estimation of the methodological error has not been precisely evaluated so far.

We here propose a method for measurement of relative CBF, OEF, and $CMRO_2$ during hyperacute ischemic stroke. The method requires two PET scans without arterial sampling, one scan for $H_2{}^{15}O$ injection and the other for $^{15}O_2$ inhalation. Regional CBF, $CMRO_2$, and OEF are determined as relative to values in a reference brain region by means of a table-lookup procedure.[9,14] In this study, we calculated "relative lookup-tables" which relate relative CBF to relative $H_2{}^{15}O$ count, relative $CMRO_2$ to relative $^{15}O_2$ count, and relative OEF to relative $^{15}O_2/H_2{}^{15}O$ count. Two assumptions were applied to the lookup-table calculation: 1) In the reference brain region, CBF and OEF were assumed to be 50.0 ml/min/100 ml and 0.40, respectively, 2) Cerebral blood volume (CBV) was assumed to be constant at 4.0 ml/100 ml over the whole brain. Errors in relative CBF, OEF and $CMRO_2$ introduced by the assumptions were estimated by a simulation study.

To examine the applicability of the present method, we compared CBF, OEF, and $CMRO_2$ measured by the present method with quantitative values using arterial sampling data for 6 chronic stroke patients. We also presented relative CBF, OEF, and $CMRO_2$ images of a hyperacute stroke patient as an example of the application, which revealed a state of "misery-perfusion".

MATERIALS AND METHODS

Model

Calculations of the PET count for the $H_2{}^{15}O$ injection were based on the single-compartment model for diffusible tracers originally developed by Kety.[15] Tissue concentration of $H_2{}^{15}O$, $C_t^{H_2O}(t)$, is described by the following equation.

$$C_t^{H_2O}(t) = fC_i(t) \otimes e^{-\frac{f}{p}t} \qquad \text{(Eq. 1)}$$

where f is a CBF, p is a partition coefficient of water in tissue to blood, and $C_i(t)$ is the arterial concentration of $H_2{}^{15}O$, which is usually measured by continuous arterial sampling for quantitative PET measurement. $\otimes$ denotes the convolution. $C_t^{H_2O}(t)$ and $C_i(t)$ are already corrected for radioactive decay. The PET count is given by integrating the tissue concentration over the scan time and is normalized to the PET count at the reference region to obtain the "relative $H_2{}^{15}O$ count," R_{H_2O}, as follows:

$$R_{H_2O} = \int_0^T C_t^{H_2O}(t)dt \Big/ \int_0^T C_{ref}^{H_2O}(t)dt \qquad \text{(Eq. 2)}$$

where T is the scan time and $C_{ref}^{H_2O}(t)$ is the concentration of $H_2{}^{15}O$ at the reference region. In the present study, the ipsilateral cerebellum was chosen as the reference region. By assuming an absolute CBF value at the reference region, R_{H_2O} can be calculated as a function of relative CBF normalized at the reference brain region, R_{CBF}. The calculated R_{H_2O} is a table of the relative $H_2{}^{15}O$ count-relative CBF relation and is called "relative lookup-table" in this article. We can determine the relative CBF from the measured relative $H_2{}^{15}O$ count by using the relative lookup-table.

For $^{15}O_2$ inhalation, the model developed by Mintun et al.[10] for the measurement of OEF and $CMRO_2$ considers $^{15}O_2$ in the vascular space and metabolized $H_2{}^{15}O$, and gives the measured activity of ^{15}O, $C_t^{O_2}(t)$, as

$$C_t^{O_2}(t) = EfC_i^O(t) \otimes e^{-\frac{f}{p}t} + VR(1 - 0.835E)C_i^O(t) + fC_i^W(t) \otimes e^{-\frac{f}{p}t} \qquad \text{(Eq. 3)}$$

where $C_i^O(t)$ and $C_i^W(t)$ are the arterial concentrations of $^{15}O_2$ and $H_2{}^{15}O$, respectively, E is an OEF, V is a CBV, and R is a small-to large-vessel hematocrit ratio. $C_t^{O_2}(t)$ consists of three components: activity of $H_2{}^{15}O$ metabolism created locally from $^{15}O_2$ extracted to the tissue, activity of unextracted ^{15}O in the vascular spaces, and activity of $H_2{}^{15}O$ by arterial recirculation of $H_2{}^{15}O$ from all tissues. The $CMRO_2$ is related to the CBF and OEF as

$$CMRO_2 = OEF \cdot CBF \cdot [O_2] \qquad \text{(Eq. 4)}$$

where $[O_2]$ is the total oxygen content of arterial blood. The PET count is given by integrating the tissue concentration over the scan time and is normalized to the PET count at the reference brain region to obtain the "relative $^{15}O_2$ count," R_{O_2}, as follows:

$$R_{O_2} = \int_0^T C_t^{O_2}(t)dt \Big/ \int_0^T C_{ref}^{O_2}(t)dt \qquad \text{(Eq. 5)}$$

where $C_{ref}^{O_2}(t)$ is the activity in the reference region. By assuming absolute CBF and OEF values at the reference region, R_{O_2} can be calculated as a function of relative $CMRO_2$ normalized at the reference region, R_{CMRO_2}. As known by Eq. 4, R_{O_2} is also a function of relative CBF and OEF. In the calculation of R_{O_2}, CBV is assumed to be constant over the whole brain. As with $CMRO_2$, "relative $^{15}O_2/H_2{}^{15}O$ count," R_{O_2/H_2O}, is calculated as a function

of relative OEF, R_{OEF}. By applying calculated R_{O_2} and R_{O_2/H_2O} called "relative lookup-table," we can determine the relative $CMRO_2$ and OEF from the measured relative $^{15}O_2$ and $^{15}O_2/H_2{}^{15}O$ counts, respectively.

Simulation Study

We performed the calculation of the relative lookup-table and the simulation study to estimate the errors of the present method. We used Eq. 1 and Eq. 3 to calculate the activity curve as a function of the time after tracer supply for various CBF and OEF. The results were integrated over the scan duration, 180 second for both Eq. 2 and Eq. 5, then converted to the relative lookup-table. p was fixed at 0.8 ml/ml in all calculations. The parameters for calculations in the reference region were fixed at 50.0 ml/min/100 ml for CBF and 0.40 for OEF. CBV was assumed to be constant at 4.0 ml/100 ml over the whole brain. The arterial activity curves used in the present calculations are shown in Figure 1. The curves for $H_2{}^{15}O$ injection and $^{15}O_2$ inhalation were described by the functions, $t\exp(-t/89.3)$ and $t^2\exp(-(t/50.7)^{1.5}) + 22.8t^{0.5}$, respectively, which reproduced well the typical arterial activity

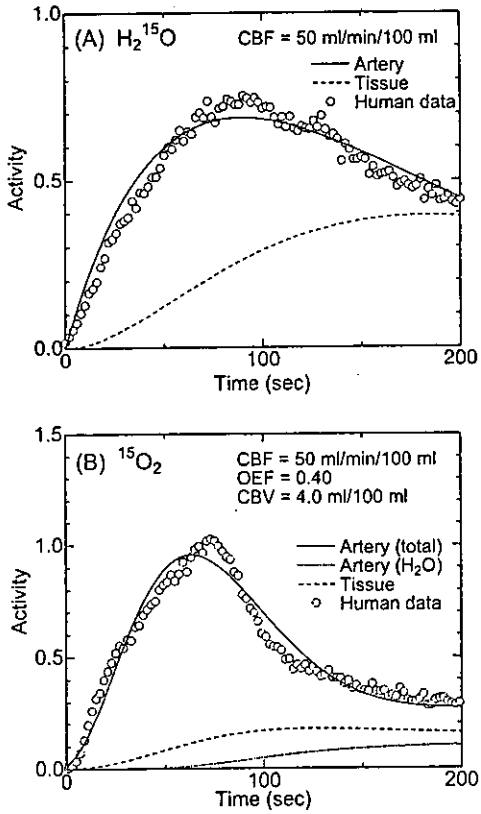

Fig. 1 The arterial activity curve used in simulations and the calculated tissue activity curve for 120 sec slow infusion of $H_2{}^{15}O$ (A) and 90 sec inhalation of $^{15}O_2$ (B) are shown. The actual human data as an example are also shown. The tissue activity was calculated under the conditions of 50.0 ml/min/100 ml for CBF, 0.40 for OEF, and 4.0 ml/100 ml for CBV. To calculate $^{15}O_2$ activity, we need the fractions of $^{15}O_2$ and $H_2{}^{15}O$ to total arterial activity; therefore, the $H_2{}^{15}O$ fraction from recirculation is also shown. The tissue activity curves were integrated from 0 s to 180 s to calculate the PET count.

Table 1 Patient information

Pat.	year/sex	vascular lesion	after onset
1	75/F	Lt. IC stenosis (>95%)	1 month
2	52/M	Lt. IC occlusion	6 months
3	71/F	Rt. IC stenosis (>90%)	asymptomatic
4	67/M	Lt. MCA stenosis	1 month
5	62/M	Rt. IC stenosis	1 month
6	70/M	Rt. IC stenosis (>80%)	3 months

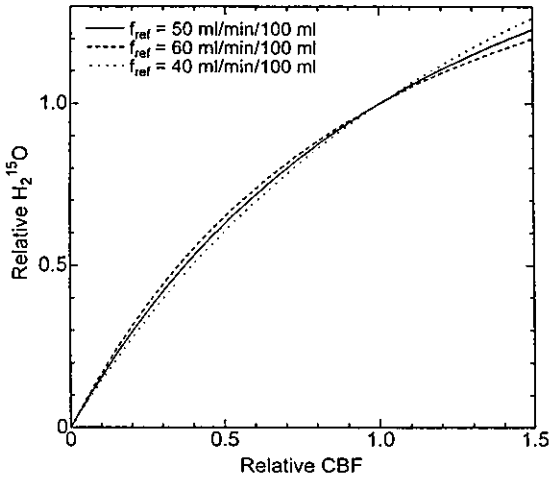

Fig. 2 Calculated relative $H_2{}^{15}O$ PET count as a function of relative CBF. Both PET count and CBF were relative values to the reference, and the reference CBF (f_{ref}) was assumed to be 50.0 ml/min/100 ml. Calculated results with reference CBF values of 40.0 and 60.0 ml/min/100 ml are also shown.

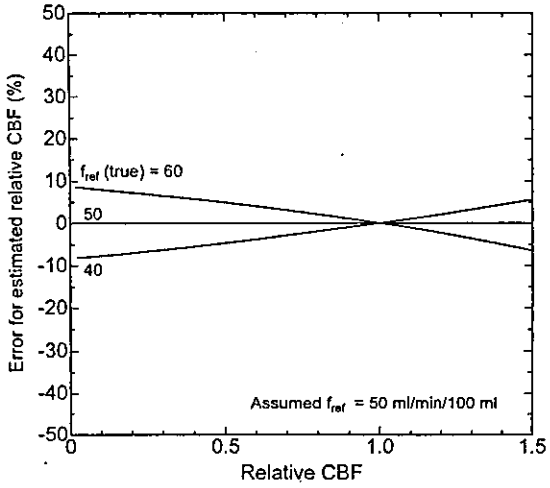

Fig. 3 Errors in the measured relative CBF by the table-lookup procedure where the reference CBF (f_{ref}) was assumed to be 50.0 ml/min/100 ml but the actual CBF (f_{ref} (true)) was 40.0 or 60.0 ml/min/100 ml.

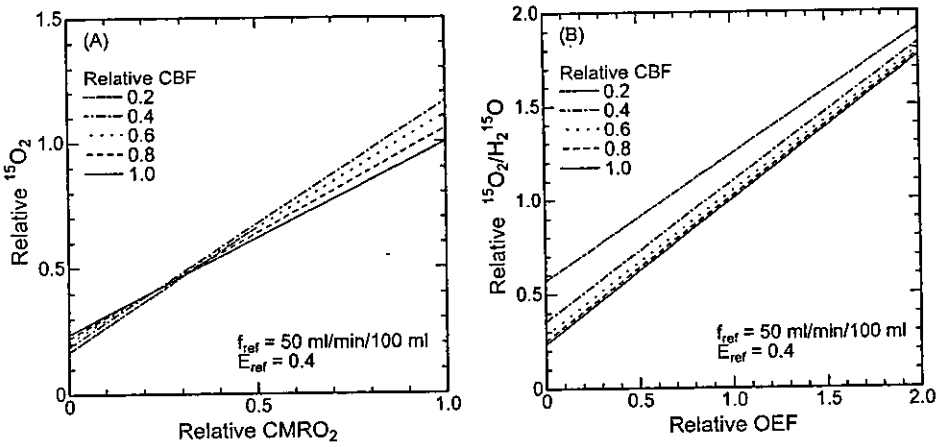

Fig. 4 Calculated relative $^{15}O_2$ (A) and $^{15}O_2/H_2{}^{15}O$ (B) PET counts as a function of relative $CMRO_2$ and OEF, respectively. For the reference region, 50.0 ml/min/100 ml CBF (f_{ref}), 0.40 OEF (E_{ref}), and 4.0 ml/100 ml CBV were assumed. The whole-brain CBV was assumed to be 4.0 ml/100 ml, the same as the reference region. The results for the relative CBF from 0.2 to 1.0 were presented.

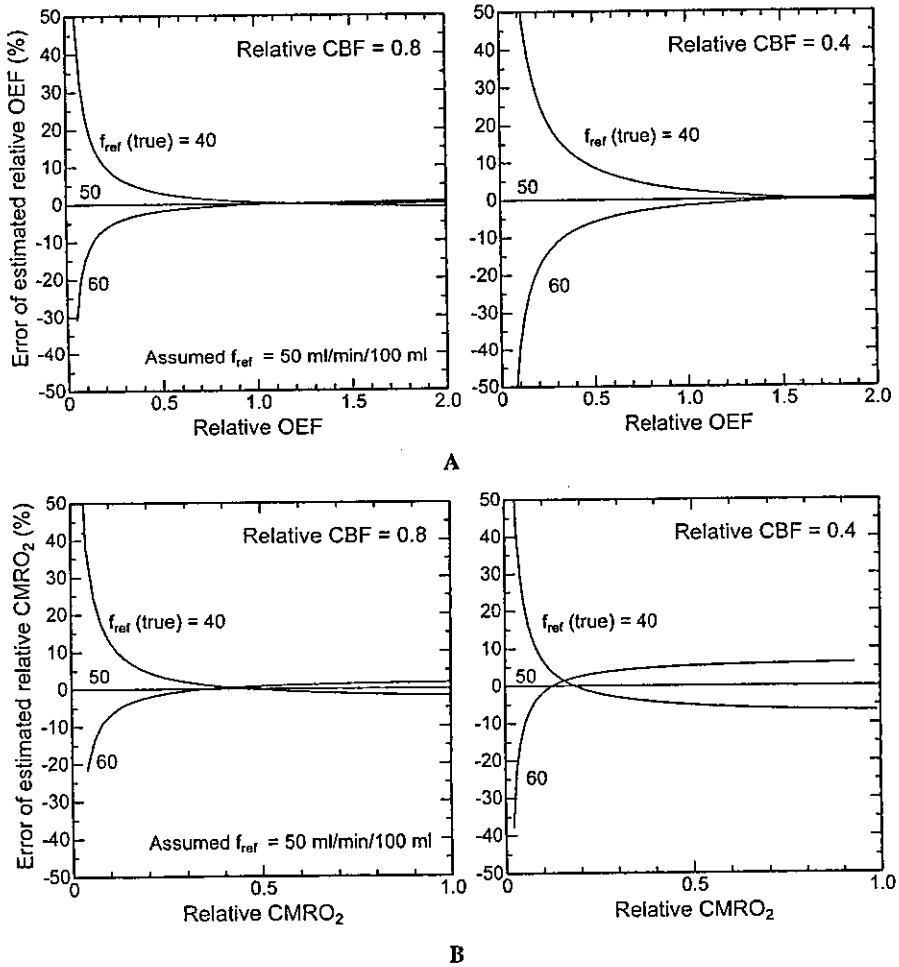

Fig. 5 Errors in measured relative OEF (A) and $CMRO_2$ (B) where the reference CBF (f_{ref}) was assumed to be 50.0 ml/min/100 ml but the actual CBF (f_{ref} (true)) was 40.0 or 60.0 ml/min/100 ml, which correspond to ±20% variations of the reference CBF. Errors are shown for two cases, when relative CBF was 0.8 (low-grade ischemia) and 0.4 (high-grade ischemia), respectively.

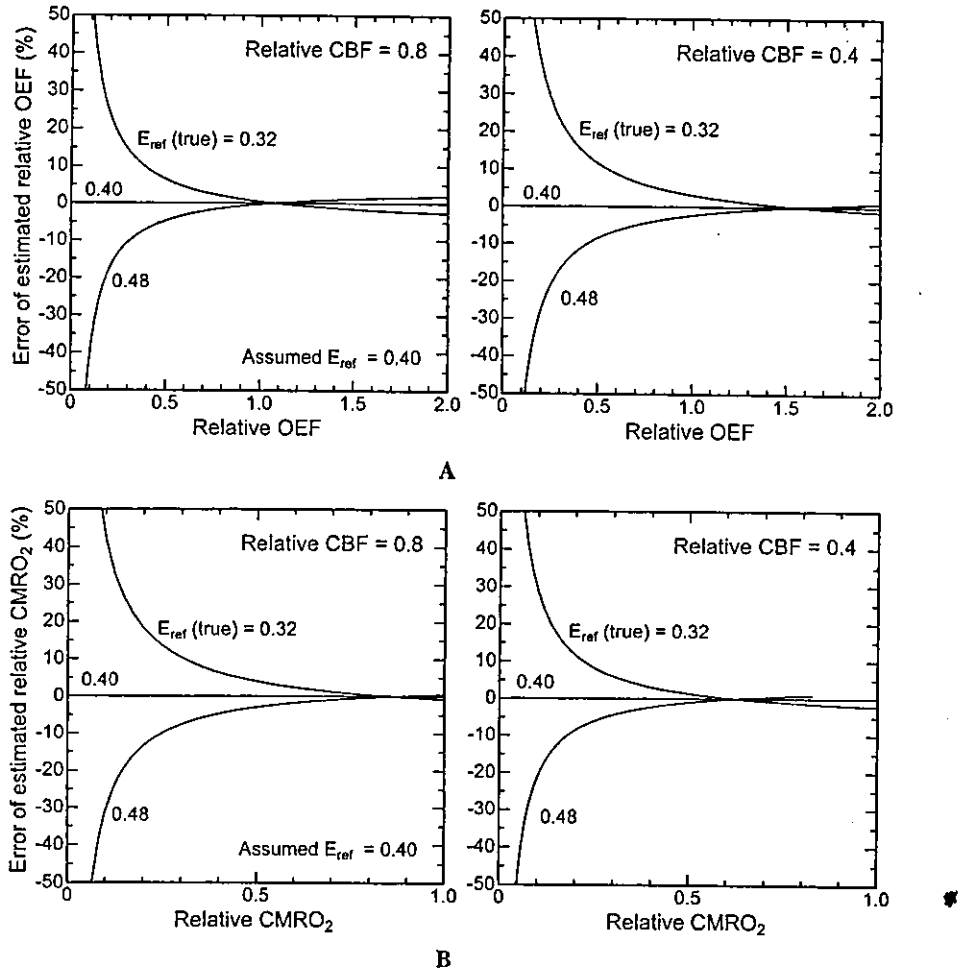

Fig. 6 Errors in measured relative OEF (A) and $CMRO_2$ (B) where the reference OEF (E_{ref}) was assumed to be 0.40 but the actual OEF (E_{ref} (true)) was 0.32 or 0.48, which correspond to ±20% variations of the reference OEF.

measured at our institute after slow infusion of $H_2{}^{15}O$ for 120 second and continuous inhalation of $^{15}O_2$ for 90 second. Figure 1 also show actual human data as an example. For $^{15}O_2$ calculations, arterial concentrations of $^{15}O_2$ and $H_2{}^{15}O$, $C_i^O(t)$ and $C_i^W(t)$ in Eq. 3, are required rather than total arterial activity. The fractions of $C_i^O(t)$ and $C_i^W(t)$ relative to the total activity were estimated according to the method of Iida et al.[16]

We next performed calculations to estimate the effects of errors in the reference parameters. The calculations were done with reference CBF values between 40.0 and 60.0 m*l*/min/100 m*l* and reference OEF values between 0.32 and 0.48, which correspond to 20% error in the assumed values. Although CBV was fixed at 4.0 m*l*/100 m*l* in the above calculations, we did other calculations in which the CBV varied between 2.0 and 6.0 m*l*/100 m*l* to estimate errors introduced by assuming a constant CBV.

Patient Study

To examine the differences between relative values by the present method and quantitative values, we performed a PET study with arterial blood sampling for 6 unilateral stroke patients in the chronic stage. The measurements were performed with a Headtome-V PET scanner,[17] and the PET procedures were the same as in the previous studies.[18,19] The patient information was summarized in Table 1. We computed two image sets for each patient, relative CBF, OEF, and $CMRO_2$ images by the present method, and absolute images by the conventional method using the blood data. CBV effects for quantitative OEF and $CMRO_2$ were corrected by PET measurements with $C\,^{15}O$ inhalation.[10,22] For relative CBF, OEF, and $CMRO_2$ images, ipsilateral cerebellum was chosen as the reference region. For region of interest (ROI) analysis to calculate lesion-contralateral hemisphere ratio of CBF, OEF, and $CMRO_2$, we picked one hypo-perfused slice for each patient. The circular ROIs with 16 mm diameter covered the cerebral cortex of the lesion and contralateral hemisphere, and lesion-contralateral ratios were calculated for each patient and each image.

We also performed PET measurement without blood sampling for a patient (67-year-old female, 4 hours after

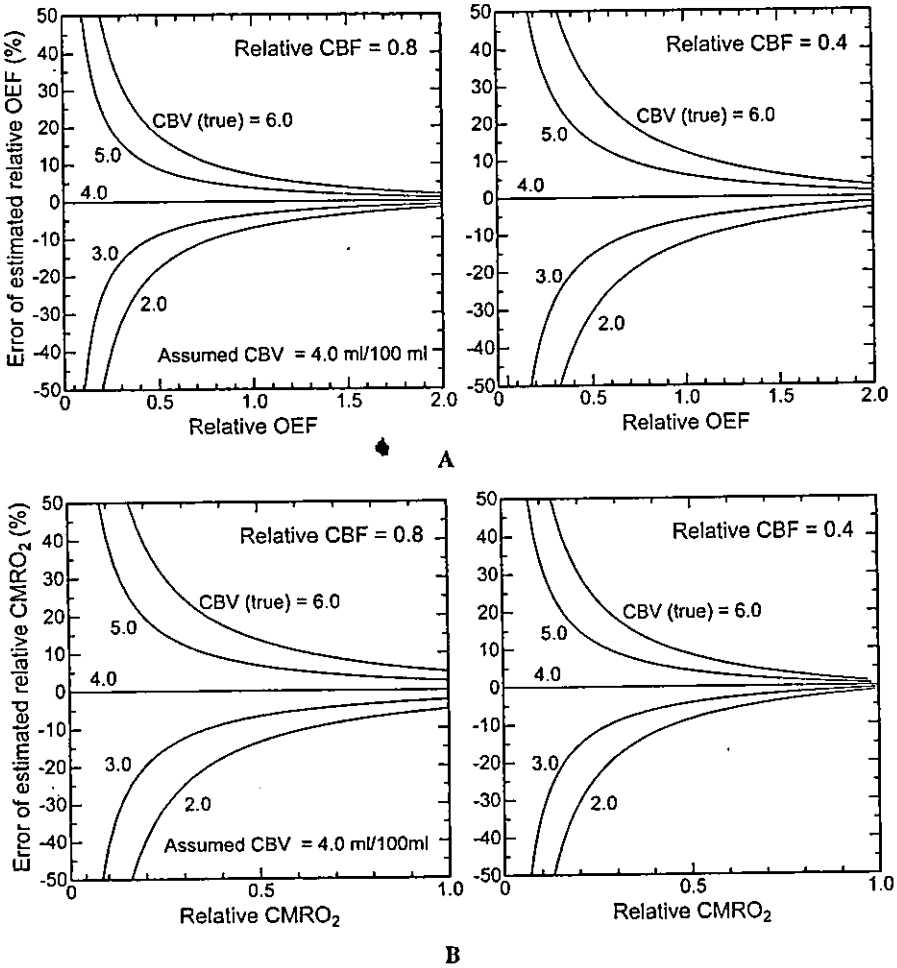

Fig. 7 Errors in measured relative OEF (A) and $CMRO_2$ (B) caused by CBV variation. The CBV was between 2.0 and 6.0 m*l*/100 m*l*, but the reference CBV was fixed at 4.0 m*l*/100 m*l*.

onset of MCA occlusion), as an example of the application for hyperacute stroke.

RESULT

Relative CBF

A calculated relative lookup-table which relates the relative $H_2{}^{15}O$ PET count (R_{H_2O}) to relative CBF (R_{CBF}) is shown in Figure 2. The reference CBF was assumed to be 50.0 m*l*/min/100 m*l*. From the relative lookup-table and the measured relative PET count, we can determine relative CBF by means of the table-lookup procedure. For example, if the relative PET count was 0.53, we can determine relative CBF to be 0.40. The lookup-tables for 40.0 and 60.0 m*l*/min/100 m*l* of the reference CBF are also shown in Figure 2. The errors in measured relative CBF resulting from the table-lookup method (reference CBF was assumed to be 50.0 m*l*/min/100 m*l*) for each case where the true reference CBF was 40.0, 50.0, or 60.0 m*l*/min/100 m*l* are shown in Figure 3. A discrepancy between the assumed and true reference CBF caused an error in the measured relative CBF, but there was no error if the assumed reference CBF was equal to the true reference CBF. For reference CBF variations between 40.0 and 60.0 m*l*/min/100 m*l*, the error was less than ±10%.

Relative $CMRO_2$ and OEF

A calculated relative lookup-table which relates the relative $^{15}O_2$ PET count (R_{O_2}) to relative $CMRO_2$ (R_{CMRO_2}) is shown in Figure 4 (*left panel*). The reference CBF and OEF values were assumed to be 50.0 m*l*/min/100 m*l* and 0.40, respectively. CBV in the whole brain was assumed to be 4.0 m*l*/100 m*l*. Because the relative $^{15}O_2$ PET count depends not only on the relative $CMRO_2$ but also on the relative CBF, the results for various relative CBF values, 1.0, 0.8, 0.6, 0.4, and 0.2, are shown. A calculated relative lookup-table which relates the relative $^{15}O_2/H_2{}^{15}O$ PET count (R_{O_2/H_2O}) to relative OEF (R_{OEF}) is shown in Figure 4 (*right panel*). The reference CBF and OEF were the same as those in the $^{15}O_2$ PET count calculations. As with relative CBF, lookup-table and measured relative PET counts allow for the determination of relative $CMRO_2$

Table 2 Lesion-contralateral ratios of CBF, OEF and $CMRO_2$ by two methods, and the ratio of the present method (relative method) to quantitative method (absolute method)

Pat.	Quantitative PET			Relative PET			Rel./Quant.		
	CBF	OEF	$CMRO_2$	CBF	OEF	$CMRO_2$	CBF	OEF	$CMRO_2$
1	0.884	1.030	0.911	0.896	1.035	0.928	1.013	1.005	1.019
2	0.830	1.073	0.886	0.844	1.073	0.902	1.018	1.000	1.018
3	0.956	1.106	1.058	0.959	1.129	1.082	1.003	1.021	1.023
4	0.831	0.905	0.749	0.833	0.901	0.746	1.002	0.995	0.996
5	0.797	1.195	0.944	0.799	1.208	0.957	1.002	1.011	1.014
6	0.800	1.044	0.836	0.800	1.042	0.836	1.001	0.998	1.000

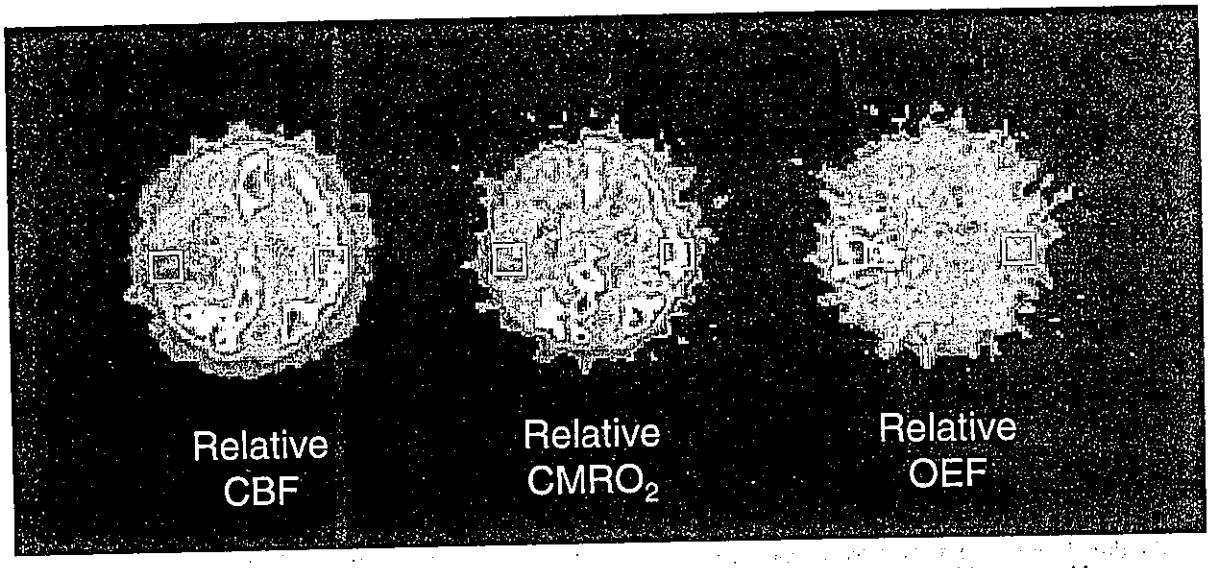

Fig. 8 Images of relative CBF (*left*), $CMRO_2$ (*center*), and OEF (*right*) from a 67-year-old woman with right middle cerebral artery occlusion. PET measurements after $H_2{}^{15}O$ injection and $^{15}O_2$ inhalation were made 4 hours after onset. Application of region of interest (ROI) markers on the lesion and the contralateral brain region is shown. Ratios of lesion to contralateral CBF, $CMRO_2$, and OEF were 0.45, 0.71 and 1.60, respectively.

and OEF. The errors of measured relative OEF (A) and $CMRO_2$ (B) where the true reference CBF was 40.0, 50.0, or 60.0 m*l*/min/100 m*l* but was assumed to be 50.0 m*l*/min/100 m*l* are shown in Figure 5. CBF of 40.0 and 60.0 m*l*/min/100 m*l* correspond to ±20% error of the assumed reference CBF (50.0 m*l*/min/100 m*l*). In Figure 5, the errors for two cases in which relative CBF was 0.8 and 0.4 corresponding to low- and high-grade ischemia, respectively, are shown. The errors of measured relative OEF caused by the inadequate assumption of the reference CBF with 20% error were smaller than 3% at relative OEF greater than 1.0 but were larger at low relative OEF values. The errors of measured relative $CMRO_2$ showed the same trends as those of relative OEF but were about ±6% at relative $CMRO_2$ values greater than 0.5 for high-grade ischemia. The errors of measured relative OEF (A) and $CMRO_2$ (B) for each case in which the true reference OEF is 0.32, 0.40, or 0.48, but is assumed to be 0.40, are shown in Figure 6. The errors of measured relative OEF and $CMRO_2$ caused by the inadequate assumption of the reference OEF with 20% error were similar and were smaller than 5% at relative OEF values greater than 1.0 and at relative $CMRO_2$ values greater than 0.5.

CBV effects on measurement of relative OEF (A) and $CMRO_2$ (B) are shown in Figure 7. The CBV varied between 2.0 and 6.0 m*l*/100 m*l* which correspond to ±50% of 4.0 m*l*/100 m*l*, but the reference CBV was fixed at 4.0 m*l*/100 m*l*. The errors of measured relative OEF increased as relative OEF and relative CBF decreased. At high OEF values (relative OEF > 1.0), relative OEF errors were less than ±8% at 0.8 of relative CBF and ±12% at 0.4 of relative CBF. In calculation of the $CMRO_2$, the magnitude of error was at the same level as that of relative OEF, but decreased as relative CBF decreased.

Patient Study

Lesion-contralateral ratios of CBF, OEF and $CMRO_2$ by two methods for 6 unilateral stroke patients in the chronic stage were summarized in Table 2. The ratio of the present method (relative method) to quantitative method

(absolute method) was also shown. The maximum difference between the two methods, 1.023, appeared in $CMRO_2$ for patient 3.

Relative CBF, $CMRO_2$, and OEF images from a 67-year-old woman with right middle cerebral artery occlusion representative of application of the present method to hyperacute stroke are shown in Figure 8. PET measurements after $H_2{}^{15}O$ injection and $^{15}O_2$ inhalation were performed 4 hours after stroke onset with a Headtome-V scanner (Shimadzu Corp., Kyoto, Japan).[17] Total measurement time including preparation and transmission scanning for attenuation correction was 30 min. Relative CBF, $CMRO_2$, and OEF in each pixel were calculated by means of the relative table-lookup method. Application of the region of interest (ROI) on the lesion and contralateral brain region is shown (Fig. 8). CBF, $CMRO_2$, and OEF values relative to the reference brain region (cerebellum) were 0.33/0.73 (lesion/contralateral side), 0.59/0.83, and 1.81/1.13, respectively. Therefore, ratios for the lesion to the contralateral side for relative CBF, $CMRO_2$, and OEF were 0.45, 0.71, and 1.60, respectively. These values indicated a state of "misery-perfusion" with CBF decreased and OEF increased to maintain the $CMRO_2$.[20]

DISCUSSION

Quantitative PET measurement of brain circulation and metabolism needs some complicated procedures, and takes more than 1 hour even for the basic examination to obtain the data of CBF, $CMRO_2$, and OEF. Arterial cannulation into the radial artery for input function measurement is the most time-consuming and invasive process, and it lengthens the total examination time of PET study. Especially in the emergency setting, examination for diagnostic imaging should be sufficiently shortened to decide the appropriate therapeutic strategy with minimization of painful procedures. We presented a method of relative PET measurement for cerebral circulation and oxygen metabolism during hyperacute stroke. Because this method is based on measurements of relative PET counts, we need only two emission scans after $H_2{}^{15}O$ injection and $^{15}O_2$ inhalation; blood samples are not needed. This makes the PET measurements simpler than the conventional quantitative measurements, shortens the scan time, and is suitable in the emergency setting for patients with hyperacute stroke. We estimated that a total measurement time of only about 30 min or less including preparation and transmission scanning would be needed. The present method provides information on "misery-perfusion" indicated by an increased OEF of the ischemic brain region, which can be measured only by PET.

In the present method, we can determine the relative CBF from the measured relative $H_2{}^{15}O$ PET count by using calculated relative lookup-table. Relative $^{15}O_2$ PET counts depend not only on relative $CMRO_2$ but also on relative CBF and OEF because $^{15}O_2$ PET count is a linear function of OEF and a nonlinear function of CBF (Eq. 3). This means that the relative $CMRO_2$ can not be determined from the relative $^{15}O_2$ PET count alone: both the relative $^{15}O_2$ and $H_2{}^{15}O$ PET counts are required. For example, when the relative $H_2{}^{15}O$ PET count of 0.53 corresponding to 0.40 for relative CBF and the relative $^{15}O_2$ PET count of 0.77 are measured, we can determine the relative $CMRO_2$ as 0.60 and the relative OEF as 1.50 by using relative lookup-table for 0.40 of relative CBF. By applying these procedures to $H_2{}^{15}O$ and $^{15}O_2$ images pixel by pixel, we can obtain relative CBF, OEF, and $CMRO_2$ images. Derdeyn et al. applied relative OEF measurements in patients with symptomatic carotid artery occlusion and looked on the relative $^{15}O_2/H_2{}^{15}O$ PET count as the relative OEF predicting the risk of stroke.[11,12] As seen in Figure 4 (*right panel*), however, there is not a one-to-one correspondence between relative $^{15}O_2/H_2{}^{15}O$ PET count and relative OEF. For example, a relative $^{15}O_2/H_2{}^{15}O$ PET count of 1.0 corresponds to a relative OEF of between 0.63 and 1.0, depending on the relative CBF. Thus, we should estimate relative OEF from the measured relative $^{15}O_2/H_2{}^{15}O$ PET count with consideration of relative CBF.

We examined the differences between the present method and conventional quantitative method for lesion-contralateral ratios of CBF, OEF, and $CMRO_2$ for chronic stroke patients. The difference between the present method (relative method) and quantitative method (absolute method) were relatively small as shown in Table 2, and within the valuation by the simulations. The maximum difference between the two methods, 1.023 of $CMRO_2$ for patient 3, was due to CBV effect. Lesion-contralateral ratio of CBV for patient 3 measured by $C^{15}O$ inhalation was about 1.2 and the highest among the patients, although these data are not shown in this article. CBF decreases in the patients were relatively mild (0.797–0.956), and therefore further study of a large number of patients with various CBF would be desirable to validate the applicability in various types of patients.

Simulations resulted in different curves depending on the value of the assumed reference CBF (Fig. 2). This was caused by the nonlinear relation between PET count and CBF. The reference CBF variation between 40.0 and 60.0 m*l*/min/100 m*l*, corresponding to ±20% variation from 50.0 m*l*/min/100 m*l*, introduced a maximum ±10% error in the measured relative CBF at its low range; larger variations will cause larger errors. In other words, we can determine the relative CBF with a less than ±10% error if variation in the reference CBF remains less than ±20%. This suggests that care must be taken when selecting the reference region. An unaffected region, such as the ipsilateral cerebellum, must be chosen to reduce errors in measured CBF.

The calculation results showed the existence of $^{15}O_2$ PET counts even if OEF equals 0. This was caused by $^{15}O_2$ activity being distributed in the vascular space that was

not extracted into the tissue space and $H_2{}^{15}O$ activity by recirculation water. This offset effect emphasized the error at low OEF and $CMRO_2$ values, but the errors rapidly decreased at higher values (Figs. 5, 6). If the main interest of the study is the detection of "misery-perfusion" in which the OEF increases to maintain $CMRO_2$ as CBF decreases, the simulations yielded positive results because the errors caused by variation of assumed CBF and OEF reference values were relatively small at high range, less than 6% at relative OEF values greater than 1.0 and relative $CMRO_2$ values greater than 0.5.

Because the present method applies only two PET scans, we can not obtain CBV which can be measured quantitatively by $C^{15}O$ inhalation.[21] In quantitative oxygen metabolism measurements, CBV is known to be one of the major error sources.[22–24] For the calculation of the relative lookup-table, we assumed a constant CBV value in whole brain. This results in identical CBV values for both the normal and affected brain region, possibly causing significant errors of measured relative $CMRO_2$ and OEF. The degree of the CBV variation in the brain of the acute stroke patient is still controversial. Powers et al. performed PET study for 7 patients with unilateral carotid artery occlusion and CBF reductions in ischemic but uninfarcted regions of brain. They reported increased CBV in regions with decreased CBF, with the CBV ratio of symptomatic to asymptomatic hemisphere of the 7 patients varying between 1.0 and 1.5.[25] Hatazawa et al. reported CBV measurement by dynamic susceptibility contrast-enhanced MRI for 9 patients with unilateral occlusion of either the middle cerebral artery or internal carotid artery within 6 hours after onset.[26] In the brain regions with mild (relative CBF > 0.60) and moderate (0.40 < relative CBF < 0.60) hypoperfusion, the mean relative CBV values were 1.29 ± 0.31 and 0.94 ± 0.49, respectively. Derdeyn et al. investigated the relationship between CBV and OEF in a large sample of patients with unilateral carotid artery occlusion enrolled in a prospective study of hemodynamic factors and stroke risk.[27] They showed that the ipsilateral-to-contralateral CBV ratio varied between 0.7 and 1.5. Based on these data, the present simulations showed the effect of CBV errors, 50% variation at 4.0 m*l*/100 m*l*. When measuring relative OEF and $CMRO_2$, lower relative CBF and OEF values will introduce larger errors. A reduction in CBF and OEF increases the ratio of the residual $^{15}O_2$ in the vascular space to that extracted into the tissue and emphasizes the CBV effects. For example, when detecting "misery-perfusion," the measured OEF errors introduced by CBV effects are less than ±8% for low-grade ischemia (0.8 of relative CBF) and ±12% for high-grade ischemia (0.4 of relative CBF). Again, we emphasize that CBV effect must be considered for the change of relative OEF in the ischemic core, whereas relative OEF in the remediable area for hyperacute thrombolytic therapy would be subject to less error by CBV effect.

CONCLUSION

We presented a method for PET measurement of relative CBF, OEF and, $CMRO_2$ with $H_2{}^{15}O$ injection and $^{15}O_2$ inhalation. The method is feasible to apply in patients with the hyperacute stage of cerebral infarction without the need for arterial sampling. In the present method, relative CBF, OEF, and $CMRO_2$ are determined by the table-lookup procedure. For the calculation of the relative lookup-table, CBF and OEF in the reference brain region were assumed to be 50.0 m*l*/min/100 m*l* and 0.40, respectively. Cerebral blood volume (CBV) was assumed to be constant at 4.0 m*l*/100 m*l* over the whole brain. For relative CBF calculation, the present simulation study revealed that 20% variation of the reference CBF value resulted in a maximum error of about 10%. CBV effects caused larger errors in measured OEF and $CMRO_2$ when CBF and/or OEF were severely decreased, mandating caution when analyzing the heavily damaged ischemic core. Sequential measurements of cerebral circulation and oxygen metabolism by the present method within a sufficiently short examination time would easily demonstrate the present salvageable area in an emergency and would have the possibility to provide useful information for application of thrombolytic or neuroprotective therapy in patients with hyperacute stroke.

REFERENCES

1. The National Institute of Neurological Disorders and Stroke rt-PA Stroke Study Group. Tissue plasminogen activator for acute ischemic stroke. *N Eng J Med* 1995; 333: 1581–1587.
2. Hacke W, Kaste M, Fieschi C, Toni D, Lesaffre E, von Kummer R, et al. Intravenous thrombolysis with recombinant tissue plasminogen activator for acute hemispheric stroke. The European Cooperative Acute Stroke Study (ECASS). *JAMA* 1995; 274: 1017–1025.
3. Shimosegawa E, Hatazawa J, Inugami A, Fujita H, Ogawa T, Aizawa Y, et al. Cerebral infarction within six hours of onset: prediction of completed infarction with technetium-99m-HMPAO SPECT. *J Nucl Med* 1994; 35: 1097–1103.
4. Ueda T, Hatakeyama T, Kumon Y, Sasaki S, Uraoka T. Evaluation of risk of hemorrhagic transformation in local intra-arterial thrombolysis in acute ischemic stroke by initial SPECT. *Stroke* 1994; 25: 298–203.
5. Ezura M, Takahashi A, Yoshimoto T. Evaluation of regional cerebral blood flow using single photon emission tomography for the selection of patients for local fibrinolytic therapy of acute cerebral embolism. *Neurosurg Rev* 1996; 19: 231–236.
6. Ueda T, Sakaki S, Yuh WT, Nochide I, Ohta S. Outcome in acute stroke with successful intra-arterial thrombolysis and predictive value of initial single-photon emission-computed tomography. *J Cereb Blood Flow Metab* 1999; 19: 99–108.
7. Frackowiak RS, Lenzi GL, Jones T, Heather JD. Quantitative measurement of regional cerebral blood flow and

Journal of Cerebral Blood Flow & Metabolism
24:188–190 © 2004 The International Society for Cerebral Blood Flow and Metabolism
Published by Lippincott Williams & Wilkins, Inc., Baltimore

Effect of Astrocytic Energy Metabolism Depressant on ^{14}C-Acetate Uptake in Intact Rat Brain

*Rie Hosoi, *Maki Okada, †Jun Hatazawa, ‡Antony Gee, and *Osamu Inoue

*From the *School of Allied Health Sciences, Faculty of Medicine, Osaka University, Osaka, Japan; the †Department of Diagnostic Medicine, Osaka University Graduate School of Medicine, Osaka, Japan; and ‡GlaxoSmithkline, Clinical Research Unit, ACCI, Addenbrookes Hospital, Cambridge, U.K.*

Summary: Fluorocitrate, a selective astrocytic toxin, was microinjected into the right striatum of rat brain, and the regional distribution of ^{14}C-acetate was measured using autoradiography. A significant reduction (more than 80%) in ^{14}C-acetate uptake over a 5-minute period was observed in the right striatum, compared with that in the left striatum (saline infused), 4 hours after fluorocitrate (1 nmol/μL) infusion. This effect was transient, and ^{14}C-acetate uptake had almost returned to normal at 24 hours after the fluorocitrate infusion. In contrast, the regional blood flow in the striatum, as determined using ^{14}C-iodoamphetamine, was significantly increased by the fluorocitrate infusion. The present observations indicate that ^{14}C-acetate uptake might be a useful characteristic for examining astrocytic energy metabolism in the intact brain. **Key Words:** ^{14}C-acetate—Astrocytic metabolism—Fluorocitrate—Rat.

Acetate has been used as a selective characteristic for examining astrocytic energy metabolism both *in vitro* and *in vivo* (Cerdan et al., 1990; Hassel et al., 1995). ^{14}C-acetate is rapidly (within minutes) incorporated into amino acids derived from the TCA cycle in the brain, producing labeled glutamine with a higher specific activity than that of glutamate, its obligatory precursor; this finding is explained by the "small" (astrocytic) pool of glutamate with a rapid turnover that is segregated from the "large" (neuronal) glutamate pool (Berl, 1973) and by the cellular localization of glutamine synthetase, mainly in astrocytic cells (Martinez-Hernandez et al., 1977). Autoradiographic or positron emission tomography (PET) studies using ^{3}H or ^{11}C-acetate have also revealed that acetate is selectively taken up into astrocytes (Muir et al., 1986) and metabolized to ^{11}C-CO_2 (Shields et al., 1992).

The selective uptake and metabolism of acetate by cultured astrocytes, compared with synaptosomes and cultured neurons, has been confirmed biochemically and appears to result from the preferential transport, but not metabolism, of acetate into astrocytes (Waniewski and Martin, 1998). The activity of acetyl-CoA synthetase, the first enzymatic step in acetate use, was greater in synaptosomes than in astrocytes, whereas acetate uptake was much more rapid in astrocytes than in synaptosomes. Using NMR, Hassel et al. (1997) also reported that blocking the astrocytic TCA cycle using fluoroacetate, which metabolite fluorocitrate inhibit aconitase in the astrocytic TCA cycle, did not prevent the entry of acetate into mouse brain. We performed an autoradiographic study using the microinjection of fluorocitrate, a selective astrocytic toxin, into the right striatum of rat brain, to determine whether the inhibition of astrocytic metabolism affects acetate uptake in intact brain and found that the fluorocitrate induced a significant reduction in ^{14}C-acetate uptake.

MATERIALS AND METHODS

Animals and chemicals

Male Wistar rats (7 to 8 weeks old) were purchased from Japan SLC (Shizuoka, Japan). The rats were housed under a 12-hour, light-dark cycle and allowed free access to food and water. All experiments on the rats were performed with the permission of the Institutional Animal Care and Use Committee, School of Allied Health Sciences, Osaka University.

DL-fluorocitric acid barium salt was obtained from Sigma-Aldrich Co. (St. Louis, MO, U.S.A.) and prepared as described by Paulsen et al. (1987). 1-^{14}C-acetate (specific activity, 2.0 GBq/mmol) was obtained from Perkin Elmer Life Science Inc (Boston, MA, U.S.A.). N-isopropylmethyl-1,3-^{14}C-p-iodoamphetamine hydrochloride (^{14}C-IMP; specific activity, 2.1 GBq/mmol) was obtained from American Radiolabeled Chemicals Inc. (St. Louis, MO, U.S.A.).

Received June 23, 2003; accepted September 11, 2003.
Address correspondence to Osamu Inoue, School of Allied Health Sciences, Faculty of Medicine, Osaka University, 1-7 Yamadaoka, Suita, Osaka 565-0871, Japan; e-mail: inoue@sahs.med.osaka-u.ac.jp.

DOI: 10.1097/01.WCB.0000098606.42140.02

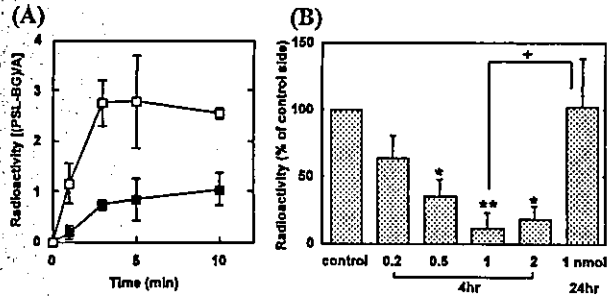

FIG. 1. (A) Time course of radioactivity concentrations in the striatum after IV injection of ^{14}C-acetate. Rats were injected with fluorocitrate (2 nmol) in the right striatum (solid square) or saline (open square) 4 hours before the tracer injection. Each value represents the mean ± SD. Significant differences were observed between the saline- and fluorocitrate-injected striatum [$F^{1,20}$ = 69.60, $P < 0.001$]. (B) Striatal uptake of ^{14}C-acetate (5 minutes) expressed as the proportion of the value on the drug-injected side to that on the saline-injected contralateral side. Each value represents the mean ± SD of 3 to 6 animals. $^{*}P < 0.05$, $^{**}P < 0.01$ *vs.* saline-injected striatum (paired *t*-test); $^{+}P < 0.05$ *vs.* fluorocitrate-injected striatum (24 hours, unpaired *t*-test).

Surgery on rat brains and infusion of fluorocitrate

The rats were anesthetized with pentobarbital (50 mg/kg, i.p.) and placed in a stereotaxic apparatus. Bilateral 26-gauge stainless steel guide cannulas fitted with 33-gauge stainless steel obturators were implanted into the striatum, according to the atlas of Paxinos and Watson (1998); 0.2 mm anterior to the bregma, 3.2 mm lateral to the midline, and 2.0 mm below the cortical surface. The guide cannulae were then fixed to the skull using stainless steel screws and acrylic cement. The rats were then allowed to recover for several days.

Fluorocitrate (0.2 to 2 nmol/μL) was infused through the infusion cannulas (33-gauge, 3.5 mm longer than the guide cannulae) and into the right striatum of each rat while the rat was awake. The infusion was performed for 4 minutes at a flow rate of 0.25 μL/min, and the infusion cannulas were left in place for an additional 3 minutes to reduce the reflux of infused drugs along the cannula track. At the same time, saline solution (1 μL) was infused into the left striatum.

In vivo autoradiography

At 4 or 24 hours after the intrastriatal drug infusion, the animals were given an intravenous bolus injection of ^{14}C-acetate (185 kBq/rat) dissolved in 0.5 mL of saline; 1, 3, 5, or 10 minutes later, the animals were killed by decapitation under a light anesthesia with diethyl ether. To measure the local cerebral blood flow, the rats were intravenously injected with ^{14}C-IMP (185 kBq/rat) dissolved in 0.5 mL of saline over a 30-second period and immediately decapitated. The brains were quickly removed and frozen. Coronal sections (20 μm) were prepared in a cryostat at −20°C and placed in contact with an imaging plate (Fuji Film Co. Ltd., Tokyo, Japan) for several days. The photo-stimulated luminescence (PSL) values in each region of the autoradiograms were then determined using the Bio-Imaging Analyzer System (BAS-1500; Fuji Photo Film). The radioactivity concentrations in regions of interest (ROIs) were expressed as (PSL-background)/area (mm^2) [(PSL-BG)/A], and the data were expressed as the proportion of the value on the drug-injected side to that on the saline-injected contralateral side.

Statistical analysis

Values were expressed as the mean ± SD (in each group), and the changes in the values compared using the Student's paired or unpaired *t*-test. Differences between the saline and fluorocitrate-treated striatum in the time course study were examined using two-way ANOVA.

RESULTS

The kinetics of ^{14}C-acetate uptake in rat striatum is shown in Fig. 1. ^{14}C-acetate was rapidly incorporated in the saline-injected striatum and reached a plateau at 3 to 10 minutes after the injection of the tracer. On the other hand, fluorocitrate (2 nmol) significantly decreased the radioactivity concentrations in the striatum. At 1 minute after the ^{14}C-acetate injection, the radioactivity level in the drug-injected striatum was less than 20% of that observed in the saline-injected striatum. Plasma radioactivity, as counted using a liquid scintillation counter, reached a maximum at 1 minute after the ^{14}C-acetate injection, and the washout at 10 minutes postinjection was less than 40% of its peak values.

The fluorocitrate (1 nmol) caused a significant reduction in ^{14}C-acetate uptake in the rat striatum 4 hours after infusion, with less than 20% of the radioactivity remaining (Figs. 1 and 2). This reduction in uptake had recovered after 24 hours, although some variation among the animals was observed. On the other hand, autoradiograms of ^{14}C-IMP 4 hours after infusion revealed a significant increase in regional blood flow in the right striatum (167 ± 57%, $P < 0.05$ *vs.* saline-injected striatum, n = 7) (Fig. 2C).

DISCUSSION

In the present study, a significant decrease in ^{14}C-acetate uptake in the striatum was observed 4 hours after the microinjection of fluorocitrate. The effect of fluorocitrate on ^{14}C-acetate uptake had almost completely disappeared 24 hours after the infusion. On the other hand, the regional blood flow in the right striatum measured with ^{14}C-IMP was significantly increased by the fluorocitrate infusion after 4 hours.

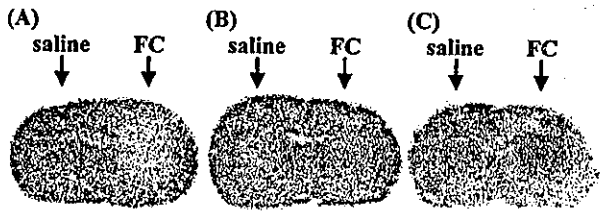

FIG. 2. Typical autoradiograms of the rat brain. (A) Incorporation of ^{14}C-acetate over a 5-minute period 4 hours after the intrastriatal infusion of fluorocitrate (FC, 1 nmol). (B) Incorporation of ^{14}C-acetate over a 5-minute period 24 hours after the intrastriatal infusion of fluorocitrate (FC, 1 nmol). (C) Incorporation of ^{14}C-IMP 4 hours after the intrastriatal infusion of fluorocitrate (FC, 1 nmol, 167 ± 57%, $P < 0.05$ *vs.* saline-injected striatum, n = 7).

Fluorocitrate has been used as a selective inhibitor of aconitase in the astrocytic TCA cycle. The intrastriatal injection of 1 nmol of fluorocitrate caused a severe reduction in the glutamine level 4 hours after the infusion, and this metabolic inhibitory effect disappeared within 24 hours (Paulsen et al., 1987). It has also been reported that fluorocitrate caused reversible ultrastructual alterations that were selective for glia (Paulsen et al., 1987). Therefore, ^{14}C-acetate uptake in the rat brain appears to occur in parallel with astrocytic energy metabolism and reflects astrocytic conditions.

The rapid uptake of ^{14}C-acetate might be mediated by monocarboxylate transporter (MCT). To date, nine members of the MCT family have been characterized (Halestrap and Price, 1999; Juel and Halestrap, 1999; Price et al., 1998); MCT1 is expressed in astrocytes, whereas MCT2 is expressed in neurons (Broer et al., 1997; Pierre et al., 2002). The time course of the radioactivities in the left striatum in this study is similar to the previous report (Berl and Frigyesi, 1969). The uptake of ^{14}C-acetate in the right (fluorocitrate-infused) striatum was significantly lower than that in the left (saline-infused) striatum at all of the time points after the injection of the tracer in this study (Fig. 1), indicating that delivery process by MCT1 was decreased or reversible transport process was promoted. Previous studies showed that the inhibition of the TCA cycle by fluoroacetate, which is metabolized to fluorocitrate that inhibits aconitase of the astrocytic TCA cycle, did not prevent the entry of acetate into mouse brain, as visualized using NMR (Hassel et al., 1997). Therefore, one possible mechanism for reduction in ^{14}C-acetate uptake in this study is the increment of both delivery and clearance caused by the higher blood flow (Fig. 2C).

Acetate can also be labeled with ^{11}C, a short half-life positron emitter, enabling astrocytic energy metabolism to be measured in living human brains using PET. To date, the 2-DG and FDG methods have been extensively developed for the study of brain metabolism *in vivo*. Whereas these procedures enable excellent regional metabolic differentiation, they cannot distinguish between neuronal and astrocytic metabolism. Such differentiation would obviously be useful in gaining a better understanding of the contribution of astrocytic metabolism to brain function and of the metabolic interactions between neurons and astrocytes. This study strongly suggested that ^{11}C-acetate may be an appropriate marker for investigating putative abnormalities in astrocytic energy metabolism in human brain disorders.

REFERENCES

Berl S, Frigyesi TL (1969) The turnover of glutamate, glutamine, aspartate and GABA labeled with [1–^{14}C]acetate in caudate nucleus, thalamus and motor cortex (cat). *Brain Res* 12:444–455

Berl S (1973) Biochemical consequences of compartmentation of glutamate and associated metabolites. In: *metabolic compartmentation in the Brain* (Balazs R and Cremer JE, eds), London: Macmillan Press, pp 3–17

Broer S, Rahman B, Pellegri G, Pellerin L, Martin JL, Verleysdonk S, Hamprecht B, Magistretti PJ (1997) Comparison of lactate transport in astroglial cells and monocarboxylate transporter 1 (MCT 1) expressing Xenopus laevis oocytes. Expression of two different monocarboxylate transporters in astroglial cells and neurons. *J Biol Chem* 272:30096–30102

Cerdan S, Kunnecke B, Seelig J (1990) Cerebral metabolism of [1,2-^{13}C2]acetate as detected by *in vivo* and *in vitro* ^{13}C NMR. *J Biol Chem* 265:12916–12926

Halestrap AP, Price NT (1999) The proton-linked monocarboxylate transporter (MCT) family: structure, function and regulation. *Biochem J* 343:281–299

Hassel B, Sonnewald U, Fonnum F (1995) Glial-neuronal interactions as studied by cerebral metabolism of [2-^{13}C]acetate and [1-^{13}C]glucose: an ex vivo ^{13}C NMR spectroscopic study. *J Neurochem* 64:2773–2782

Hassel B, Bachelard H, Jones P, Fonnum F, Sonnewald U (1997) Trafficking of amino acids between neurons and glia *in vivo*. Effects of inhibition of glial metabolism by fluoroacetate. *J Cereb Blood Flow Metab* 17:1230–1238

Juel C, Halestrap AP (1999) Lactate transport in skeletal muscle - role and regulation of the monocarboxylate transporter. *J Physiol* 517:633–642

Martinez Hernandez A, Bell KP, Norenberg MD (1977) Glutamine synthetase: glial localization in brain. *Science* 195:1356–1358

Muir D, Berl S, Clarke DD (1986) Acetate and fluoroacetate as possible markers for glial metabolism *in vivo*. *Brain Res* 380:336–340

Paulsen RE, Contestabile A, Villani L, Fonnum F (1987) An *in vivo* model for studying function of brain tissue temporarily devoid of glial cell metabolism: the use of fluorocitrate. *J Neurochem* 48:1377–1385

Paxinos G, Watson C (1998) *The Rat Brain in stereotaxic coordinates 4th edition*, San Diego: Academic Press

Pierre K, Magistretti PJ, Pellerin L (2002) MCT2 is a major neuronal monocarboxylate transporter in the adult mouse brain. *J Cereb Blood Flow Metab* 22:586–595

Price NT, Jackson VN, Halestrap AP (1998) Cloning and sequencing of four new mammalian monocarboxylate transporter (MCT) homologues confirms the existence of a transporter family with an ancient past. *Biochem J* 329:321–328

Shields AF, Graham MM, Kozawa SM, Kozell LB, Link JM, Swenson ER, Spence AM, Bassingthwaighte JB, Krohn KA (1992) Contribution of labeled carbon dioxide to PET imaging of carbon-11-labeled compounds. *J Nucl Med* 33:581–584

Waniewski RA, Martin DL (1998) Preferential utilization of acetate by astrocytes is attributable to transport. *J Neurosci* 18:5225–5233

JOURNAL OF NEUROTRAUMA
Volume 21, Number 7, 2004

Pp. 923–931

Src Family Kinase Inhibitor PP1 Reduces Secondary Damage after Spinal Cord Compression in Rats

CHIHIRO AKIYAMA,[1] TAKAMICHI YUGUCHI,[2] MASAMI NISHIO,[1] TAKAHIRO TOMISHIMA,[1] TOSHIYUKI FUJINAKA,[1] MASAAKI TANIGUCHI,[1] YOSHIKAZU NAKAJIMA,[1] EIJI KOHMURA,[3] and TOSHIKI YOSHIMINE[1]

ABSTRACT

The synthetic pyrazolopyrimidine, 4-amino-5-(4-methylphenyl)-7-(t-butyl)pyrazolo[3,4-d]pyrimidine (PP1) is a novel, potent, and selective inhibitor of Src family tyrosine kinases. Vascular permeability appears to be mediated by vascular endothelial growth factor (VEGF), which requires the activation of downstream Src family kinases to exert its function. This study investigates the effects of PP1 on vascular permeability and inflammatory response in a rat spinal cord compression model. Ten minutes after compression, PP1 (PP1 group) or the vehicle only (control group) was administered. On days 1, 3, and 7 after compression, the spinal cords were removed and examined histopathologically to determine the expression of VEGF and the extent of edema and inflammation. The dry-weight method was used to measure the water content of the spinal cords. The mRNA levels of tumor necrosis factor a (TNFα) and interleukin 1β (IL-1β), which is related to inflammatory responses, were measured with a real-time polymerase chain reaction (RT-PCR) system 6 h after compression. Although VEGF expression was similar in both groups, the extent of contusional lesion in the PP1 group was reduced by approximately 35% on day 3. Moreover, the water content on days 1, 3, and 7 was significantly reduced and macrophage infiltration on days 3 and 7 was dramatically reduced in the PP1 group. TNFα and IL-1β mRNA expression in the PP1 group were also significantly reduced. These results indicate that PP1 reduces secondary damage after spinal cord injury.

Key words: edema; macrophage infiltration; PP1; secondary damage; spinal cord injury; Src family kinase inhibitor

INTRODUCTION

Following spinal cord injury, vascular permeability increases around the area of the injury, which may lead to both edema formation and inflammation eventually progressing to secondary tissue damage (Orlicek et al., 1999; Earnhardt et al., 2002). Controlling vascular permeability and inflammatory responses therefore, may be important for the attenuation of secondary damage. Vascular endothelial growth factor (VEGF) is involved in the aggravation of secondary damage after spinal cord injury (Sköld et al., 2000). VEGF is a well-known spe-

[1]Department of Neurosurgery, Osaka University Medical School, Suita, Japan.
[2]Department of Neurosurgery, Spine and Spinal Cord Center, Yukioka Hospital, Osaka, Japan.
[3]Department of Neurosurgery, Kobe University Graduate School of Medicine, Kobe, Japan.

cific endothelial mitogen associated with angiogenesis (Lennmyr et al., 1998), as well as a potent mediator of vascular permeability (Senger et al., 1983). VEGF is reported to be involved in brain edema associated with tumors (Plate and Risau, 1995), cerebral infarction (Cobbs et al., 1998), and neurotrauma (Papavassiliou et al., 1997).

VEGF works through the activation of Src family kinases, that are located downstream in the VEGF signal transduction pathway (Eliceiri et al., 1999). Src family kinases mediate signaling in response to a variety of growth factors, including VEGF (Schlessinger, 2000), and they contribute to, among others, angiogenesis, stimulation of cell survival, and acceleration of vascular permeability.

The synthetic pyrazolopyrimidine, 4-amino-5-(4-methylphenyl)-7-(t-butyl)pyrazolo[3,4-d]pyrimidine (PP1) is a novel, potent, and selective inhibitor of Src family tyrosine kinases (Hanke et al., 1996). A recent study found that PP1 significantly reduced the size of infarction in a mouse middle cerebral artery (MCA) occlusion model (Paul et al., 2001).

On the basis of these findings, we hypothesized that the inhibition of Src family kinases by PP1 may lead to the reduction of edema formation and inflammatory responses caused by various forms of neurotrauma. In this study, we examined the effects of PP1 on vascular permeability and inflammatory responses in a rat spinal cord compression model.

MATERIALS AND METHODS

Spinal Cord Compression Model

All animal experiments were conducted in compliance with the *NIH Guide for the Care and Use of Laboratory Animals* (1996) and the *Osaka University Medical School Guidelines for the Care and Use of Laboratory Animals.* Surgical and experimental procedures were approved by the Osaka University Medical School Animal Care and Use Committee.

Forty female Wistar rats (age = 8 weeks, body weight = 200 g) were used for this model, because urinary management of female rats was considered easier than that of males. The rats were anesthetized with an intraperitoneal injection of pentobarbital (60 mg/kg) and placed in the prone position. A vertical linear incision was made along the midline of the back, followed by a single segmental laminectomy over Th10 to expose the dura of the spinal cord. A Sugita temporary clip with a calibrated closing force of 70 g (Mizuho Co., Ltd., Tokyo, Japan) was applied over the dura to compress the spinal cord for 3 sec. The skin was then closed and the animals were returned to their cages. During surgery, rectal temperature was maintained at ~36–37°C with a controlled heating pad.

PP1 (Biomol Research Laboratories, Plymouth Meeting, PA), suspended in 30% dimethyl sulfoxide (DMSO) with 0.01 M phosphate-buffered saline (PBS; He et al., 2000), was administered intraperitoneally 10 min after spinal cord compression (PP1 group) following the methods of Paul et al. (2001). The dosage used was 1.5 mg/kg weight to ensure that the maximum effect was achieved with this dosage (Paul et al., 2001). For the control group, the vehicle alone was administered using the same procedure.

Histological Procedure

On days 1, 3, and 7 after compression, rats from the two groups were deeply anesthetized with an intraperitoneal injection of pentobarbital (100 mg/kg). Their spinal cords were rapidly removed and immediately covered with Tissue-Tek embedding medium (Sakura Finetek, Torrance, CA), frozen at −80°C in 2-methylbutane, and stored at that temperature until further processing. Sagittal serial cryostat sections were cut at a thickness of 10 μm and then processed for either hematoxylin and eosin (HE) staining or immunohistochemistry (Bartholdi et al., 1997).

HE staining was used to estimate the extent of the damage. With the use of Scion image analysis software for Windows (1998; Scion Corporation, Frederick, MD), the extent of contusional lesion on day 1 after compression was calculated as the area where the color intensity of eosin had decreased by more than 50% in sagittal sections containing the central canal. On days 3 and 7, the area of inflammatory cell infiltration around the contusional area was also included in the calculation of the contusion's extent. This measurement was performed for three consecutive sections from each rat.

Immunohistochemical Staining

Immunohistochemical staining of VEGF, IgG, and ED-1 was performed to examine respectively, the expression of VEGF, the extent of edema, and the extent of macrophage infiltration. Immunohistochemical staining was done according to the method of Fujinaka et al. (2003), with some modifications.

Sections were fixed with 4% paraformaldehyde in 0.1 M phosphate buffer for 45 min, permeated with methanol at −20°C for 10 min, and finally incubated with 3% hydrogen peroxidase for 30 min to quench endogenous peroxidase. The sections were rinsed in PBS and nonspecific protein binding was blocked with 2% normal horse serum in a buffer (0.1% Triton X-100 and 5% sucrose in

PBS) for 20 min. Incubation with the primary antibodies was carried out at 4°C overnight.

The primary antibodies used for this procedure were anti-VEGF mouse monoclonal antibody (Santa Cruz Biotechnology, Santa Cruz, CA; diluted 1:100) and anti-ED-1 mouse monoclonal antibody (Serotec, Kidlington, Oxford, UK; diluted 1:100). To detect binding of the primary antibodies to the corresponding antigens, the sections were first incubated with the biotinylated anti-mouse IgG antibody (Vector Laboratories, Burlingame, CA; diluted 1:200) at room temperature for 30 min and then with abidin-biotin peroxidase complex (Vectastain Elite ABC kit, Vector Laboratories) for 30 min. The end product was visualized by means of a 3,3′-diamino-benzidine tetrahydrochloride (DAB) and hydrogen peroxidase solution and counterstained with hematoxylin. Control immunostaining consisted of the omission of the primary antibody from the immunostaining protocol.

The procedure for anti-IgG rabbit polyclonal antibody (Vector Laboratories; diluted 1:200) differed somewhat from the method described above in that the sections were incubated with 2% normal rabbit serum for 20 min, followed by incubation with this antibody at room temperature for 30 min, and finally with the abidin-biotin peroxidase complex for 30 min. The other procedures were the same as described above.

Scion image for Windows was used to define the extent of ED-1 positive cell infiltration as the area where more than 10 ED-1–positive cells were observed under high magnification (×400) in the sagittal section containing the central canal. These measurements were performed for three consecutive sections from each rat.

Determination of Water Content after Spinal Cord Compression

As another method to assess edema, the spinal cords obtained on days 1, 3, and 7 after compression under deep anesthesia were cut into lengths of 3 cm in the rostrocaudal direction, centering to the compression site. The spinal cords of nonoperated, normal animals served as normal controls. The wet weight of the spinal cords was measured immediately after their removal, after which the cords were dried at 100°C for 72 h and their dry weight determined (Suzuki et al., 2002). The water content was calculated using the following equation: water content (%) = [(wet weight − dry weight)/wet weight] × 100 (Paczynski et al., 2000).

Quantification of TNFα and IL-1β mRNA Levels in the Injured Spinal Cord

To investigate the magnitude of the inflammatory response, tumor necrosis factor a (TNFα) mRNA and interleukin 1β (IL-1β) mRNA expression were measured with a real-time polymerase chain reaction (RT-PCR) system. This technique facilitates the quantification of complementary DNA (cDNA) amplification and involves a fluorescence-based RT-PCR followed by measurement of the amplification with the ABI PRISM 7700 Sequence Detection System (Applied Biosystems, Foster, CA).

RT-PCR analysis was performed as reported elsewhere (Ueno et al., 2001). Briefly, total RNA was purified from 30 mg of each injured spinal cord obtained 6 h after compression using the RNA Easy Mini Kit (Qiagen, Hilden, Germany), according to the manufacturer's instructions. For this procedure, genomic DNA was dissolved by DNase I treatment and RNA samples were frozen in liquid nitrogen and stored at −80°C until use.

First-strand cDNA synthesis from the RNA samples was carried out using the SuperScript First-Strand Synthesis System for RT-PCR (Invitrogen Corp., Carlsbad, CA). cDNA synthesis was performed in triplicate, and for each cDNA synthesis, 200 ng of mRNA in 8 μL of water was incubated with 1 μL of oligo-d(T) primer (0.5 μg/μL) and 1 μL of dNTP mix (10 mM) at 65°C for 5 min. The solution was briefly chilled on ice, and then added to 2 μL of 10 × RT buffer, 4 μL of 25 mM $MgCl_2$, 2 μL of 0.1 M DTT, and 1 μL of RNase Out Recombinant RNase Inhibitor. After incubation at 42°C for 2 min, 1 μL (50 units) of SuperScript II reverse transcriptase was added to each tube. The reaction was incubated at 42°C for 60 min, followed by 70°C for 15 min to terminate the reaction. After the reactant had been collected by means of brief centrifugation, 1 μL of RNase H was added to each tube and incubated at 37°C for 20 min to dissolve the residual RNA. Parallel reactions for each RNA sample were run in the absence of SuperScript II reverse transcriptase to detect the presence of any contaminating genomic DNA (no RT samples). Following synthesis, cDNA was aliquoted into microtiter plates in preparation for TaqMan RT-PCR.

For each PCR, 1 μL of cDNA was used and each transcript was measured in triplicate. The RT-PCR technique is based on the hydrolysis of a specific fluorescent probe at each amplification cycle by the 5′-endonuclease activity of Taq polymerase. We used the technique as described by Depre et al. (1998) and Medhust et al. (2000), with some modifications. Predeveloped TaqMan Assay reagents (Applied Biosystems) were used for the probes and primers for TNFα and IL-1β in quantities of 200 nmol/L for each PCR as recommended by the manufacturer. PCR was then performed with 40 cycles of naturing at 95°C for 15 sec and annealing at 60°C for 1 min. Due to the relative lack of precision of spectrophotometric measurements of RNA concentration, the level of transcripts for the cellular enzyme glyceraldehyde 3-